Rapid evaluation of notch stress intensity factors using the peak stress method with 3D tetrahedral finite element models: Comparison of commercial codes

RAPID EVALUATION OF NOTCH STRESS INTENSITY FACTORS USING THE PEAK STRESS METHOD WITH 3D TETRAHEDRAL FINITE ELEMENT MODELS: COMPARISON OF COMMERCIAL CODES

G. Meneghetti[1*], A. Campagnolo[1], A. Visentin[1], M. Avalle[2], M. Benedetti[3], A. Bighelli[3], D. Castagnetti[4], A. Chiocca[5], L. Collini[6], M. De Agostinis[7], A. De Luca[8], E. Dragoni[4], S. Fini[7], V. Fontanari[3], F. Frendo[5], A. Greco[9], G. Marannano[10], F. Moroni[6], A. Pantano[10], A. Pirondi[6], A. Rebora[2], A. Scattina[11], R. Sepe[9], A. Spaggiari[4], B. Zuccarello[10]

[1] Department of Industrial Engineering, University of Padova, Via Venezia, 1 – 35131 Padova (Italy)
[2] Department of Mechanical, Energy, Management and Transportation Engineering, University of Genova, Via all'Opera Pia, 15 - 16145 Genova (Italy)
[3] Department of Industrial Engineering, University of Trento, Via Sommarive, 9 - 38123 Povo, Trento (Italy)
[4] Department of Sciences and Methods for Engineering, University of Modena and Reggio Emilia, Via Amendola 2 - 42122 Reggio Emilia (Italy)
[5] Department of Civil and Industrial Engineering, University of Pisa, Largo L. Lazzarino 2 - 56122 Pisa (Italy)
[6] Department of Engineering and Architecture, University of Parma, Parco Area delle Scienze 181/A - 43124 Parma (Italy)
[7] Department of Industrial Engineering, University of Bologna, Viale del Risorgimento, 2 – 40136 Bologna (Italy)
[8] Department of Engineering, University of Campania "Luigi Vanvitelli" Via Roma, 29 81031 Aversa, CE, Italy
[9] Department of Industrial Engineering, University of Salerno, Via G. Paolo II, 132, 84084 Fisciano, Italy
[10] Dipartimento di Ingegneria, Università di Palermo, Viale delle Scienze, 90128 Palermo, Italia
Engineering Department, University of Palermo, Viale delle Scienze, 90128 Palermo Italy
[11] Department of Mechanical and Aerospace Engineering, Politecnico di Torino, Corso Duca degli Abruzzi, 24 - 10129 Torino (Italy)

[*]Corresponding author: giovanni.meneghetti@unipd.it, tel. 0039 049 8276751, fax 0039 049 8276785

ABSTRACT
The Peak Stress Method (PSM) allows a rapid application of the notch stress intensity factor (NSIF) approach to the fatigue life assessment of welded structures, by employing the linear elastic peak stresses evaluated by FE analyses with coarse meshes. Because of the widespread adoption of 3D modelling of large and complex structures in the industry, the PSM has recently been boosted by including four-node and ten-node tetra elements of Ansys FE software, which allows to discretize complex geometries. In this paper, a Round Robin among eleven Italian Universities has been performed to calibrate the PSM with seven different commercial FE codes. Accordingly, several 3D mode I, II and III problems have been analysed. Finally, the PSM has been calibrated for given stress analysis conditions in terms of: (i) FE code, (ii) element type, (iii) mesh pattern and (iv) procedure to extrapolate stresses at FE nodes.

Keywords: Notch Stress Intensity Factor (NSIF), Peak Stress Method (PSM), FE Analysis, Coarse Mesh, Tetrahedral element.

NOMENCLATURE

a	characteristic dimension of a sharp V-notch, i.e. the minimum between the notch depth and the ligament size
d	element size of a coarse mesh pattern to apply the peak stress method (PSM)
E	material Young's modulus
K_1, K_2, K_3	notch stress intensity factors (NSIFs) relevant to mode I, II and III loadings
K^{*}_{FE}, K^{**}_{FE}, K^{***}_{FE}	non-dimensional parameters to estimate K_1, K_2 and K_3 by using the peak stress method (PSM)
r, θ, z	cylindrical coordinates
U_r, U_θ, U_z	displacement components in the cylindrical coordinate system
U_x, U_y, U_z	displacement components in the Cartesian coordinate system
x, y, z	Cartesian coordinates

Symbols

2α	opening angle of the considered sharp V-notch
λ_1, λ_2, λ_3	stress singularity degrees relevant to mode I, II and III loadings
ν	material Poisson's ratio

$\sigma_{11,peak}$	singular, linear elastic, maximum principal stress computed at the sharp V-notch tip by FE analysis according to the PSM
$\sigma_{ij,c}^{(I)}$	centroidal stress component, where I = finite element number
$\sigma_{ij,k}^{(I)}$	nodal stress component, where k = node number, I = finite element number
$\sigma_{ij,k}$	nodal stress component, where k = node number
$\overline{\sigma}_{ij,peak}$	moving average of the peak stresses computed on three adjacent vertex nodes of a FE mesh consisting of tetra elements
σ_{rr}, $\sigma_{\theta\theta}$, $\tau_{r\theta}$	normal and in-plane shear stress components in a cylindrical reference system
$\sigma_{\theta\theta,\theta=0,peak}$	singular, linear elastic, opening (mode I) peak stress computed at the sharp V-notch tip by FE analysis according to the PSM
$\tau_{r\theta,\theta=0,peak}$	singular, linear elastic, in-plane shear (mode II) peak stress computed at the sharp V-notch tip by FE analysis according to the PSM
τ_{rz}, $\tau_{\theta z}$	out-of-plane shear stress components in a cylindrical reference system
$\tau_{\theta z,\theta=0,peak}$	singular, linear elastic, anti-plane shear (mode III) peak stress computed at the sharp V-notch tip by FE analysis according to the PSM
$[\sigma]_k^{(I)}$	nodal stress tensor, where k = node number, I = finite element number
$[\sigma]_k$	stress tensor, where k = node number

Abbreviations

FEM	Finite element method
LEFM	Linear Elastic Fracture Mechanics
NSIF	Notch stress intensity factor
PSM	Peak stress method
SED	Strain energy density
SIF	Stress intensity factor
TCD	Theory of Critical Distances

1. INTRODUCTION

In the context of the fatigue design of welded components, design codes and recommendations[1,2] suggest several methods, namely the nominal stress[3,4], the structural hot-spot stress[3–7], the notch stress[3,4,8–17] and the Linear Elastic Fracture Mechanics (LEFM)[3,9,15,17–20] approaches. Additionally, criteria based on local parameters, such as stress, strain or strain energy, proved to be reliable for fatigue design of welded components, especially when complex welded details or load conditions are considered[12,21–23]. Among these, the most widely adopted are based on Notch Stress Intensity Factors (NSIFs)[24–27], averaged strain energy density (SED)[15,26–29], critical plane concepts[21,22,30] and the Theory of Critical Distances (TCD)[11,22,31,32]. The NSIF-based approach assumes the worst-case geometry both at the weld toe and at the weld root of the joint, which are idealised as sharp V-notches having null tip radius (ρ = 0) and opening angles of 135° and 0°, respectively, as highlighted in Fig. 1a. The NSIFs permit to quantify the intensity of the singular, linear elastic stress fields close to a sharp V-notch tip. As an example, Fig. 1b shows the mode I, II and III local stress components acting at the weld toe of a partial-penetration tube-to-flange welded joint subjected to a combined bending and torsion loading. Williams[33] first derived analytically the singular, linear elastic stress field ahead of a sharp V-notch tip under mode I and II loadings. Afterwards, Qian and Hasebe[34] determined the singular stress distributions due to sharp V-notches subjected to mode III loading. Later on, Gross and Mendelson[35] defined the mode I, II and III NSIF-terms by means of Eqs. (1), (2) and (3), respectively:

$$K_1 = \sqrt{2\pi} \cdot \lim_{r\to 0}\left[\left(\sigma_{\theta\theta}\right)_{\theta=0} \cdot r^{1-\lambda_1}\right] \quad (1)$$

$$K_2 = \sqrt{2\pi} \cdot \lim_{r\to 0}\left[\left(\tau_{r\theta}\right)_{\theta=0} \cdot r^{1-\lambda_2}\right] \quad (2)$$

$$K_3 = \sqrt{2\pi} \cdot \lim_{r\to 0}\left[\left(\tau_{\theta z}\right)_{\theta=0} \cdot r^{1-\lambda_3}\right] \quad (3)$$

In previous expressions the terms λ_1, λ_2 and λ_3 represent the stress singularity degrees[33,34], which depend on the V-notch opening angle 2α. Values of λ_1, λ_2 and λ_3 referring to some notch opening angles, i.e. 2α = 0°, 90°, 120° and 135°, are listed in Table 1. It is worth mentioning that the mode II stresses are not singular for notch opening angles 2α > 102° as demonstrated in Refs.[33,36], which very often simplifies the analysis at the weld toe where 2α =135°. Finally, the stress components in Eqs. (1)-(3) are referred to a cylindrical reference system (see Fig. 1b) centred at the V-notch tip, where the z-direction is tangent to the notch tip line and the θ-direction is aligned with the notch bisector line, r being the radial coordinate. Accordingly, $\sigma_{\theta\theta}$, $\tau_{r\theta}$ and $\tau_{\theta z}$ are calculated ahead of the notch tip ($r\to 0$) and along the notch bisector line (θ=0).

NSIF-parameters have been widely adopted in the literature to correlate the fatigue strength of arc-welded joints undergoing uniaxial[24,37–39] or multiaxial[25] loading conditions. Nevertheless, it should be noted that the calculation of NSIF-terms on the basis of the results of numerical analyses shows a major drawback in engineering applications, since very refined FE meshes (finite element size on the order of 10^{-5} mm were adopted for 2D numerical analyses in Ref. [24]) are required in order to apply Eqs. (1)-(3). When dealing with three-dimensional, complex and large-scale notched structures, both the solution of the FE model and the post-processing of numerical results could be even more time-consuming. To overcome this drawback, an engineering and rapid technique, the Peak Stress Method (PSM), has been proposed to speed up the calculation of the NSIF-terms by adopting coarse FE analyses, the element size being some orders of magnitude larger than that required to apply Eqs. (1)-(3). The PSM takes inspiration from the contribution by Nisitani and Teranishi[40], who proposed a technique to readily estimate the mode I Stress Intensity Factor (SIF) of a crack propagating from an ellipsoidal cavity. The PSM has been first justified theoretically and later on extended to allow the rapid calculation also of the NSIF relevant to sharp and open V-notches under mode I[41,42], the SIF of cracks under mode II[43] and, finally, the NSIF of open V-notches under mode III[44].

Practically, the PSM is a numerical tool, which takes advantage of the opening, in-plane shear and out-of-plane shear peak stresses evaluated from a linear elastic FE analysis with coarse mesh (see an example in Fig. 2) to rapidly estimate the NSIF-terms K_1, K_2 and K_3, respectively, according to the following expressions[41,43,44]:

$$K_1 \cong K_{FE}^{*} \cdot \sigma_{\theta\theta,\theta=0,peak} \cdot d^{1-\lambda_1} \tag{4}$$

$$K_2 \cong K_{FE}^{**} \cdot \tau_{r\theta,\theta=0,peak} \cdot d^{1-\lambda_2} \tag{5}$$

$$K_3 \cong K_{FE}^{***} \cdot \tau_{\theta z,\theta=0,peak} \cdot d^{1-\lambda_3} \tag{6}$$

where $\sigma_{\theta\theta,\theta=0,peak}$, $\tau_{r\theta,\theta=0,peak}$ and $\tau_{\theta z,\theta=0,peak}$ are the peak stresses calculated with respect to a local cylindrical coordinate system, which must be centred at the node located at the V-notch tip and have *z*-direction tangent to the notch tip line and θ-direction aligned with the notch bisector line, *r* being the radial direction. The subscript 'θ=0' defines the direction along which peak stresses have to be calculated; as an example $\sigma_{\theta\theta,\theta=0,peak}$ represents the opening stress acting normal to the notch bisector, as highlighted in Fig. 2. The parameter *d* is the average finite element size adopted by the free mesh generation algorithm available in the FE code. Finally, K^{*}_{FE}, K^{**}_{FE} and K^{***}_{FE} are coefficients which must be calibrated to account for[45]: (i) the element type and integration scheme; (ii) the free mesh pattern and (iii) the procedure adopted by the FE code to extrapolate the stresses at nodes.

The PSM according to Eqs. (4)-(6) has been calibrated in previous investigations by employing several 2D and 3D element types and commercial FE codes. First, the parameters K^{*}_{FE}, K^{**}_{FE} and K^{***}_{FE} have been calibrated by using 2D, four-node plane quadrilateral elements of Ansys Mechanical APDL element library[41,43,44]. Subsequently, a Round Robin Project was run[45] to calibrate the coefficients K^{*}_{FE} and K^{**}_{FE} for 2D, four-node plane quadrilateral elements available in six commercial FE packages other than Ansys Mechanical APDL, namely Abaqus, Straus7, MSC Patran/Nastran, LUSAS, HyperMesh/OptiStruct/HyperView, and HyperMesh/LS-Dyna/HyperView. A further development consisted in extending the PSM to 3D, eight-node brick elements[42], by taking advantage of the submodeling technique of Ansys® FE software. More precisely, when considering a complex 3D welded structure, first a main model having a free-mesh of ten-node tetra elements is solved and then a submodel of the critical region is meshed with a regular pattern of eight-node brick elements and eventually analysed with the PSM.

Given the ever increasing adoption of three-dimensional modelling of large-scale complex structures in the industry, the 3D PSM has recently been improved by calibrating coefficients K^{*}_{FE}, K^{**}_{FE} and K^{***}_{FE} for four-node and ten-node tetra elements[46,47] of Ansys Mechanical APDL element library. These finite element types allow to easily discretize complex three-dimensional geometries and to apply the PSM directly to the free-meshed main model, making the submodel with regular mesh pattern unnecessary. Nevertheless, mesh patterns consisting of tetra elements are typically irregular, in the sense that each node belonging to the notch tip line can be shared by a different number of elements and have significantly different sizes and shapes (see for example next Fig. 10). As a consequence, the peak stress components could vary along the notch tip line, even in cases where the NSIF-parameters are constant. To smooth the peak stress distribution along the notch tip line, the average peak stress has been introduced and defined as the moving average of peak stresses evaluated on three adjacent vertex nodes[46]. For example, the average peak stress at node n=k is calculated as:

$$\overline{\sigma}_{ij,peak,n=k} = \left. \frac{\sigma_{ij,peak,n=k-1} + \sigma_{ij,peak,n=k} + \sigma_{ij,peak,n=k+1}}{3} \right|_{n=node} \tag{7}$$

Therefore, the PSM-coefficients K^{*}_{FE}, K^{**}_{FE} and K^{***}_{FE} have been calibrated in[46,47] by adopting four-node and ten-node tetra elements and by input the average peak stress components according to Eq. (7) into Eqs. (4)-(6), i.e. $\overline{\sigma}_{\theta\theta,\theta=0,peak}$, $\overline{\tau}_{r\theta,\theta=0,peak}$ and $\overline{\tau}_{\theta z,\theta=0,peak}$ in place of the peak stresses $\sigma_{\theta\theta,\theta=0,peak}$, $\tau_{r\theta,\theta=0,peak}$ and $\tau_{\theta z,\theta=0,peak}$, respectively. Furthermore, Fig. 2 highlights that: (i) the PSM based on tetra elements cannot be applied at nodes laying on a free surface of the considered notched structure[46,47], since peak stress values at those nodes are affected by the distorted mesh pattern; (ii) peak stresses

must be calculated only at vertex nodes of ten-node tetra elements; i.e. peak stresses existing at mid-side nodes must be neglected.
The comparison between Eqs. (4)-(6) and previous Eqs. (1)-(3) shows that the PSM has a further advantage in addition to the coarse FE mesh: only a single linear-elastic peak stress evaluated at the singularity location is necessary to estimate each NSIF-term, instead of a number of *stress versus distance* results, which require a post-processing analysis.
Incidentally, thanks to Eqs. (4)-(6), any NSIF-based approach for the structural strength assessment of notched structures can in principle be reformulated on the basis of the PSM. Recently, the PSM has been applied in combination with the approach based on the averaged strain energy density (SED) to assess the fatigue strength of welded joints under axial[43,48], torsion[44] and multiaxial[49,50] loading conditions. For additional details, the reader is referred to the recent state-of-the-art reviews focused on NSIF[51], averaged SED[52,53] and PSM[54] approaches.
To broaden the possibility of using the 3D PSM with 3D tetrahedral finite element models, it is of paramount importance to calibrate the parameters K^{*}_{FE}, K^{**}_{FE} and K^{***}_{FE} for commercial FE packages other than Ansys. Therefore, following the track of the previous Round Robin[45] focused on the 2D PSM, the present investigation presents the results of a new Round Robin which has been performed to determine K^{*}_{FE}, K^{**}_{FE} and K^{***}_{FE} for 3D tetrahedral finite element models. To the best of authors' knowledge, the 3D PSM based on tetra elements of FE codes other than Ansys has been adopted only in a recent paper[55], where the NSIFs resulting from welding residual stresses have been rapidly estimated in steel butt-welded joints using Sysweld.
The work plan of the present Round Robin consisted in applying the PSM to several 3D V-notch problems under pure mode I, pure mode II and pure mode III loadings by adopting four-node or ten-node tetra elements available in different FE software packages. After having evaluated the peak stresses from the FE models and the average peak stresses according to Eq. (7), the non-dimensional parameters K^{*}_{FE}, K^{**}_{FE} and K^{***}_{FE} have been calculated using Eqs. (4), (5) and (6), but now rearranged in the following way:

$$K^{*}_{FE} \cong \frac{K_1}{\overline{\sigma}_{\theta\theta,\theta=0,peak} \cdot d^{1-\lambda_1}} \tag{8}$$

$$K^{**}_{FE} \cong \frac{K_2}{\overline{\tau}_{r\theta,\theta=0,peak} \cdot d^{1-\lambda_2}} \tag{9}$$

$$K^{***}_{FE} \cong \frac{K_3}{\overline{\tau}_{\theta z,\theta=0,peak} \cdot d^{1-\lambda_3}} \tag{10}$$

For each numerical software package, the calibration has been carried out by keeping fixed the following analysis conditions: (i) element type and integration scheme, (ii) free mesh pattern and (iii) procedure to extrapolate stresses at nodes.

2. CALIBRATING THE PSM WITH 3D TETRAHEDRAL ELEMENTS OF ANSYS® MECHANICAL APDL FE CODE

The PSM parameters K^{*}_{FE}, K^{**}_{FE} and K^{***}_{FE} appearing in Eqs. (4), (5) and (6) have been calibrated using tetrahedral elements of Ansys Mechanical APDL in a previous paper[47], which the reader is referred to. The obtained values are recalled in next Table 4, as a function of the loading mode, the element type and the notch opening angle, while the conditions of applicability are summarised in the following:

- the following tetrahedral elements of Ansys Mechanical APDL element library have been calibrated:
  - three-dimensional, four-node, linear tetrahedral elements (SOLID 285);
  - three-dimensional, ten-node, quadratic tetrahedral elements (SOLID 187);
- Eq. (4) and (6) can be adopted to analyse sharp V-notches under mode I and III, respectively, having an opening angle $0° \le 2\alpha \le 135°$. On the other hand, Eq. (5) can be applied to analyse the crack problem ($2\alpha = 0°$) under mode II loading, while in a recent paper[54] it has been extended to treat also the case $2\alpha = 90°$, which is the typical case of a weld root with a gap.
- the average size d of the tetra elements defining the free mesh pattern can be chosen within the range of applicability reported in Table 4 in terms of minimum mesh density ratio a/d, adopted element type and notch opening angle. a represents the characteristic size of the considered sharp notch, e.g. a is the notch depth in Fig. 3c; more precisely, a is the minimum between the V-notch depth and the ligament size (indicated as h in Fig. 3). In the great majority of the notch problems considered in the present study, the characteristic size a corresponded to the notch depth since $a < h$; however, few exceptions exist in Table 3 for which $a > h$; however, to simplify the presentation of the results, a has been always adopted to identify the notch depth also in these cases.

- To apply the 3D PSM with Ansys Mechanical APDL FE code, the 'FULL graphics' option must be activated before evaluating the peak stresses in the post-processing environment.

3. FE CODES AND PARTICIPANTS INVOLVED IN THE ROUND ROBIN

Table 2 summarises the seven FE software packages and the eleven participants involved in the Round Robin. It is worth noting that LS-Dyna and Optistruct have been employed as solvers, while Hypermesh and Hyperview have been adopted as pre-processor and post-processor enviroments, respectively.

4. GEOMETRIES, MATERIAL AND FE MESH PATTERNS

Three-dimensional mode I, II and III notch problems have been analysed by adopting different FE codes. The considered geometries include cracks as well as sharp V-notches and not necessarily represent welded components, due to the general validity of expressions (4)-(6) to be calibrated. On one hand, geometries, material parameters, element types, constraint and loading conditions have been obviously kept the same in all FE software. On the other hand, as far as possible, specific settings relevant to element formulations, mesh generation algorithms and procedures to extrapolate and to average stress components at FE nodes have been set to *default options* in each FE code. In the Discussion section, to investigate the reasons for the different obtained results, additional FE analyses of the following types have been performed: (i) a FE software has been adopted enforcing the default criterion regarding the stress extrapolation at nodes of another FE code; (ii) the mesh pattern generated by a given FE code has been imported into another code in order to compare the results keeping the same FE mesh pattern. All details relevant to the FE analyses carried out and the post-processing of the results are reported in the following. As a general setting for all analyses, linear elastic, static structural analyses have been performed and a structural steel having Young's modulus E = 206000 MPa and Poisson's ratio ν = 0.3 has been adopted.

4.1 3D problems (plane strain), mode I loading, 2α = 0°, 90°, 120°, 135°

A number of 3D notch problems under pure mode I loading as sketched in Figs. 3a-d have been analysed, all geometries being the same treated in the original calibration of the PSM based on tetra elements carried out using Ansys Mechanical APDL code[47]. More in detail, the following case studies have been considered: a crack (2α = 0°) at the tip of a U-notch (Fig. 3(a)); a plate with lateral cracks (2α = 0°) (Fig. 3(b)); a plate with lateral sharp V-notches (2α = 90°, 120°, 135°) (Fig. 3(c)) and the weld toe (2α = 135°) of a full-penetration cruciform welded joint (Fig. 3(d)).
Three-dimensional analyses have been performed by adopting a mesh pattern of four-node or ten-node tetra elements, see the examples in Fig. 3a-d, which refer to Ansys Mechanical APDL code. The free mesh generation algorithm available in each FE code has been executed, after having set the desired FE size *d*. The mesh density ratio *a/d* has been varied in the range between 1 and 13, by considering several values of notch/crack size *a* and element size *d,* as summarised in Table 3. One eighth of each geometry has been modelled by exploiting the triple symmetry condition; plane strain conditions have been simulated by constraining the out-of-plane displacement U_z according to Figs. 3a-d, resulting in $\varepsilon_z = 0$. A pure mode I axial load has been applied to each FE model by means of a nominal gross-section tensile stress equal to 1 MPa.
After solution of the FE analyses, the opening peak stress $\sigma_{\theta\theta,\theta=0,peak}$ has been evaluated at vertex nodes belonging to the crack or V-notch tip lines (see Figs. 3a-d). In all considered FE codes, stress averaging at FE nodes has been activated, so that only a single value of $\sigma_{\theta\theta,\theta=0,peak}$ has been obtained per node, i.e. the average of the nodal stresses from all elements sharing the node. To do this, the *default options* of each FE software have been employed, as it will be discussed in the next sections. After that, Eq. (7) has been applied to calculate the average peak stress $\overline{\sigma}_{\theta\theta,\theta=0,peak}$ at each vertex node.

The exact values of the NSIF K_1, to be employed in Eq. (8), have been computed by adopting Ansys Mechanical APDL code and by applying Eq. (1) to the stress-distance results obtained from two-dimensional FE analyses under plane strain conditions. Very refined FE meshes of eight-node, quadratic quadrilateral elements (PLANE 183 of Ansys® element library), having size of the order of 10^{-5} mm close to the notch tip, have been employed.

4.2 3D problems (plane strain), mode II loading, 2α = 0°

A crack (2α = 0°) centred in a plate (Fig. 3e) has been analysed under pure mode II loading conditions, the geometry being taken from the original calibration of the PSM based on tetra elements performed with Ansys Mechanical APDL code[47].
Three-dimensional analyses have been carried out by using a free FE mesh of four-node or ten-node tetra elements, see the example of Fig. 3e, which refers to Ansys Mechanical APDL code. A mesh density ratio *a/d* in the range from 1 to 25 has been adopted, as shown in Table 3. Only one eighth of the cracked plate has been modelled taking advantage of the double anti-symmetry condition on planes YZ and XZ and of the symmetry condition on plane XY (see Fig. 3e); plane

strain conditions have been simulated by constraining the out-of-plane displacement U_z according to Fig. 3e. Pure mode II shear has been applied to each FE model by means of displacements $U_x = U_y = 1.262 \cdot 10^{-3}$ mm at the plate free lateral surfaces, which correspond to a nominal gross-section shear stress equal to 1 MPa in the corresponding crack-free geometry.
After solution, the in-plane shear peak stress $\tau_{r\theta,\theta=0,peak}$ has been evaluated at vertex nodes belonging to the crack tip line (Fig. 3e), stress averaging at FE nodes being activated as explained above when dealing with mode I problems. Eventually, Eq. (7) has been employed to calculate the average peak stress $\overline{\tau}_{r\theta,\theta=0,peak}$ at each vertex node.

Again, the exact values of the SIF K_2, to be employed in Eq. (9), have been calculated by adopting Ansys Mechanical APDL code and by applying Eq. (2) to the stress-distance results derived from two-dimensional FE analyses with very refined FE meshes of eight-node, quadratic quadrilateral elements (PLANE 183 of Ansys® element library), under plane strain conditions.

4.3 3D problems, mode III loading, 2α = 0°, 90°, 120°, 135°

Different 3D notch problems subjected to pure mode III loading as sketched in Figs. 3f-h have been analysed. All geometries are the same considered in the original calibration of the PSM based on tetra elements performed using Ansys Mechanical APDL code[47]. The following case studies have been treated: a circumferential crack (2α = 0°) or sharp V-notch (2α = 90°, 120°, 135°) in a cylindrical bar (Fig. 3(f)); a sharp V-notch (2α = 90°, 120°, 135°) at a shaft shoulder (Fig. 3(f)) and the weld root (2α = 0°) in a geometry that recalls that of a tube-to-tube welded joint (Fig. 3(h)).
Three-dimensional analyses have been performed by employing a free mesh pattern of either four-node or ten-node tetra elements, see the examples in Fig. 3f-h, referred to Ansys Mechanical APDL code. The mesh density ratio *a/d* has been varied in the range between 1 and 10, as summarised in Table 3. A 90°-segment of each cylindrical geometry has been modelled taking advantage of the double anti-symmetry condition on planes YZ and XY. Moreover, the anti-symmetry on plane XZ as well has been also employed for the geometry of Fig. 3f; conversely, dealing with geometries of Figs. 3g,h, the free face on plane XZ has been fully constrained. Finally, two tangential forces F_θ have been applied at nodes located at the opposite face to generate a pure mode III torsion load, translating into a nominal shear stress, referred to the section having diameter Φ, equal to 1 MPa.
After solution, the out-of-plane shear peak stress $\tau_{\theta z,\theta=0,peak}$ has been evaluated at vertex nodes belonging to the crack or V-notch tip lines (Figs. 3f-h), stress averaging at FE nodes being activated as described for mode I FE analyses. Then, Eq. (7) has been used to calculate the average peak stress $\overline{\tau}_{\theta z,\theta=0,peak}$ at each vertex node.

Again, the exact values of the NSIF K_3, to input in Eq. (10), have been calculated by using Ansys Mechanical APDL code and by applying Eq. (3) to the stress-distance results derived from two-dimensional FE analyses with very refined FE meshes of eight-node, quadratic quadrilateral harmonic elements (PLANE 83 of Ansys® element library).

5. DETAILS OF MESH GENERATION SETTINGS

Three-dimensional free mesh patterns consisting of four-node or ten-node tetra elements have been adopted in the FE analyses. Table 2 shows that the four-node tetra element has been integrated using 1 Gauss point, Ansys Mechanical APDL being the only exception since it employs 4 Gauss points; on the other hand, the ten-node tetra element has been integrated using 4 Gauss points by all considered FE codes. To run the free mesh generation algorithm, first, the proper element type has been selected, then, the sole parameter, which the FE analyst has input, has been the average element size *d*. More details regarding the element type selection and the adopted mesh generation settings in individual FE codes have been summarised in Appendix A.

6. RESULTS OF FE ANALYSES

Figures 4, 5 and 6 report the results obtained from the participants in the Round Robin regarding the mode I, mode II and mode III notch problems, respectively. The results are expressed in terms of the PSM parameters K^*_{FE}, K^{**}_{FE} and K^{***}_{FE}, defined by Eqs. (8), (9) and (10), respectively, as a function of the mesh density ratio *a/d*. It should be noted that, the variability of the average peak stress $\overline{\sigma}_{ij,peak}$ along the notch or crack tip lines causes a non-uniform distribution of coefficients K^*_{FE}, K^{**}_{FE} and K^{***}_{FE} in each FE model. Therefore, Figs. 4, 5 and 6 report the mean value of the non-dimensional parameters K_{FE} evaluated from each FE model as well as the relevant bar, which represents the range between maximum and minimum K_{FE} values evaluated along each notch or crack tip line. In the case of the same FE code adopted by different participants (see for example the number of users of Ansys Mechanical APDL in Table 2), the mean value and the bar of the ratios K_{FE} reported in Figs. 4, 5 and 6 have been calculated collecting together the numerical results of all users. It is worth noting that the results generated by the same FE code adopted by different users are interesting for the present Round Robin, since the mesh pattern generated for a given geometrical case could change by varying the order

of creation of the geometrical entities or the performances of the adopted PC. Such differences of the FE mesh patterns and of the corresponding peak stresses are taken into account by the bars of the ratios K_{FE} reported in Figs. 4, 5 and 6.
Figs. 4-6 show that, for a given element type, the majority of the adopted FE software present similar values of the non-dimensional parameters K^{*}_{FE}, K^{**}_{FE} and K^{***}_{FE} and of the minimum mesh density ratio *a/d* for the applicability of the PSM. More in detail, concerning 3D, four-node tetra elements, Figs. 4, 5 and 6 highlight that:

- Under mode I loading (see Fig. 4), K^{*}_{FE} is in the range between 1.68 and 1.78 for all considered values of the notch opening angle 2α, the deviation being between ±18% and ±30%. Convergence is obtained when $a/d \geq 1$.
- Dealing with mode II loading (see Fig. 5), K^{**}_{FE} is in the range between 2.63 and 3.00, the deviation being between ±12% and ±18%, and convergence is obtained when the ratio $a/d \geq 3$.
- Concerning mode III loading, the obtained results are reported in Fig. 6, which shows that K^{***}_{FE} is in the range between 2.35 and 2.60, the deviation being between ±15% and ±23%, and convergence is obtained when the ratio $a/d \geq 5$.

Dealing with 3D, ten-node tetra elements, Figs. 4, 5 and 6 highlight that:

- Under mode I loading, Fig. 4 show that K^{*}_{FE} is in the range between 1.05 and 1.07, with a deviation between ±15% and ±23%, for 2α equal to 0°, 90° or 120°. K^{*}_{FE} is in the range between 1.20 and 1.21, with a deviation between ±8% and ±12%, when 2α equals 135°. The only exceptions are FE packages Hypermesh/LS-Dyna/Hyperview and Hypermesh/Optistruct/Hyperview which present K^{*}_{FE} = 1.84±24% and 1.80±22%, respectively, for all considered values of the notch opening angle 2α. Convergence is obtained when $a/d \geq 1$ for all cases.
- Concerning mode II loading (see Fig. 5), K^{**}_{FE} is in the range between 1.61 and 1.63, with a deviation between ±13% and ±20%, while convergence is obtained for a ratio $a/d \geq 1$. Again, the only exceptions are Hypermesh/LS-Dyna/Hyperview and Hypermesh/Optistruct/Hyperview which present a K^{**}_{FE} = 2.70±18% and 2.87±15% and convergence is obtained when $a/d \geq 3$.
- Dealing with mode III loading, Fig. 6 show that K^{***}_{FE} is in the range between 1.32 and 1.40, with a deviation between ±10% and ±15%, for 2α equal to 0° and 90°, convergence being obtained for a ratio $a/d \geq 3$, the only exception being Abaqus for which it must be $a/d \geq 5$. On the other hand, K^{***}_{FE} is in the range between 1.60 and 1.70, with a deviation between ±10% and ±12%, when 2α equals 120° or 135°, convergence being obtained for a ratio $a/d \geq 1$, the only exception being again Abaqus for which it must be $a/d \geq 4$. Once again, Hypermesh/LS-Dyna/Hyperview and Hypermesh/Optistruct/Hyperview present different values of the PSM parameters, namely K^{***}_{FE} = 2.45±15% for $a/d \geq 3$ and K^{***}_{FE} = 2.50±18% for $a/d \geq 1$, respectively, for all considered values of the notch opening angle 2α.

Table 4 summarises all results showed in Figs. 4, 5 and 6, i.e. the non-dimensional ratios K^{*}_{FE}, K^{**}_{FE} and K^{***}_{FE} to input in Eqs. (4), (5) and (6) and the minimum mesh density ratio *a/d* for individual FE software packages.
Importantly, the PSM parameters K^{*}_{FE}, K^{**}_{FE} and K^{***}_{FE} reported here using Ansys Mechanical APDL are slightly different results as compared to the original calibration[47], as it can be observed from Table 4. In fact, the mean values of the parameters K_{FE} have been slightly modified and a little greater deviation has to be accepted to take into account the distribution of the results obtained by all users of Ansys Mechanical APDL, due to the different mesh pattern generated for a given geometry; on the other hand, the minimum mesh density ratio *a/d* to achieve convergence has been reduced. See for example the case of mode I notch problems treated with four-node tetra elements: according to the original calibration[47] it resulted K^{*}_{FE} = 1.75±22% for $a/d \geq 3$, while the present calibration provides K^{*}_{FE} = 1.70±30% for $a/d \geq 1$.
Figures 4-6 show that the calibration of the K^{*}_{FE}, K^{**}_{FE} and K^{***}_{FE} performed using Solidworks provides different results as a function of the adopted mesh generation option, i.e. *standard* or *blend*. More in detail, results generated using *standard mesh* are highly scattered, especially for mode II crack problems (see Fig. 5), while results obtained using a *blend mesh* are consistent with those generated by the other FE codes. This is due to the generated mesh pattern, which is quasi-mapped, consisting of right triangles on the free surface of the component, for the *standard mesh*, while it is free, i.e. made of nearly equilateral triangles, when using the *blend mesh*, as sketched in Table 2. Accordingly, the scatter bands reported in Figs. 4-6 and the results summarized in Table 4 relevant to Solidworks have been referred only to the *blend mesh*, which is consistent with the mesh patterns generated by the other FE codes, which typically define a free mesh pattern of predominantly equilateral triangles.
Finally, the different calibration constants obtained using Hypermesh/LS-Dyna/Hyperview and Hypermesh/Optistruct/Hyperview, depend on criteria for stress extrapolation at FE nodes and will be discussed in the following section.

7. DISCUSSION

In previous section, some differences have been observed among the results provided by the adopted FE software packages. The most significant one is highlighted by Figs. 4-6 and Table 4 and is that Hypermesh/LS-Dyna/Hyperview and Hypermesh/Optistruct/Hyperview deliver K^{*}_{FE}, K^{**}_{FE} and K^{***}_{FE} values calculated with ten-node tetra elements

completely different from those found with all other FE codes. Other minor differences of PSM coefficients provided by the other FE codes have also been observed. Such discrepancies have been motivated on the basis of the different criteria adopted to extrapolate stresses at FE nodes, of the generated mesh patterns and of the finite element formulations, as reported in more detail in the following sections.

7.1 Stress extrapolation at FE nodes

Numerical results are calculated by FE software at the Gauss (or integration) points of each finite element. Then, results can be evaluated at nodal or centroidal locations by employing the relevant shape functions. The stress component can be calculated at a node shared by different elements by adopting two criteria, as reported in Fig. 7 referred to a node shared by two elements[56,57]:

(a) The nodal stresses in the element ($\sigma_{ij,k}^{(I)}$ and $\sigma_{ij,k}^{(II)}$ in Fig. 7a) are derived by extrapolating the stresses existing at the Gauss points. Then, the nodal stresses per element are averaged to compute the stress component at the node ($\sigma_{ij,k}$ in Fig. 7a):

$$\sigma_{ij,k}=\frac{\sigma_{ij,k}^{(I)}+\sigma_{ij,k}^{(II)}}{2} \quad \text{or in the general case} \quad \sigma_{ij,k}=\frac{\sum_{n=1}^{N}\sigma_{ij,k}^{(n)}}{N} \quad N=\#\text{ FEs sharing node k} \tag{11}$$

(b) The centroidal stresses in the element ($\sigma_{ij,c}^{(I)}$ and $\sigma_{ij,c}^{(II)}$ in Fig. 7b) are derived by interpolating the stresses existing at the Gauss points and, then, they are attributed to the shared node. Afterwards, they are averaged to compute the stress component at the shared node ($\sigma_{ij,k}$ in Fig. 7b):

$$\sigma_{ij,k}=\frac{\sigma_{ij,c}^{(I)}+\sigma_{ij,c}^{(II)}}{2} \quad \text{or in the general case} \quad \sigma_{ij,k}=\frac{\sum_{n=1}^{N}\sigma_{ij,c}^{(n)}}{N} \quad N=\#\text{ FEs sharing node k} \tag{12}$$

The procedure sketched in Fig. 7a and defined in Eq. (11) is applied by the great majority of the adopted FE codes, i.e. Ansys, Abaqus, Lusas and Solidworks. On the other hand, the postprocessor Hyperview allows to apply either Eq. (11) or Eq. (12); however, both solvers LS-Dyna and Optistruct do not compute nodal stresses in the element, therefore Hyperview can apply only procedure of Fig. 7b and Eq. (12) for stress extrapolation at nodes. This explains why the PSM parameters K^{*}_{FE}, K^{**}_{FE} and K^{***}_{FE} delivered by LS-Dyna and Optistruct are different from those derived using the other FE software packages, as highlighted in Figs. 4-6 and in Table 4. This conclusion has been validated by recalibrating the coefficients K^{*}_{FE}, K^{**}_{FE} and K^{***}_{FE} using Ansys Mechanical APDL FE code, but enforcing the use of Eq. (12) to extrapolate stresses at FE nodes. The obtained results are reported in Fig. 8, which includes also the results previously generated by LS-Dyna and Optistruct (Figs. 4-6) and the scatter bands calibrated on LS-dyna results. Figure 8 shows that enforcing Eq. (12), Ansys Mechanical APDL FE software provides K_{FE} values consistent with those obtained using Hypermesh/LS-Dyna/Hyperview and Hypermesh/Optistruct/Hyperview.

7.2 Principal stress averaging

When considering a pure opening (mode I) notch problem, the PSM can be applied through Eq. (4) by adopting the maximum principal stress $\sigma_{11,peak}$, which is approximately equal to the opening peak stress $\sigma_{\theta\theta,\theta=0,peak}$ but easier to evaluate, because it does not require a properly aligned cylindrical coordinate system.

Starting from the nodal stress tensors per element calculated with any criterion mentioned previously (Eq. (11) or Eq. (12)), the principal stresses at a node shared by different finite elements can be evaluated according to two averaging procedures, as sketched in Fig. 9 for a node shared by two elements:

(a) The nodal stress tensors per element ($[\sigma]_k^{(I)}$ and $[\sigma]_k^{(II)}$ in Fig. 9a) are averaged at the share node ($[\sigma]_k$ in Fig. 9a). Then, the nodal principal stress is evaluated ($\sigma_{11,k}$ in Fig. 9a).

(b) The nodal principal stress per element ($\sigma_{11,k}^{(I)}$ and $\sigma_{11,k}^{(II)}$ in Fig. 9b) is calculated from the relevant nodal stress tensors per element ($[\sigma]_k^{(I)}$ and $[\sigma]_k^{(II)}$ in Fig. 9b). Afterwards, nodal principal stress ($\sigma_{11,k}$ in Fig. 9b) is obtained by averaging the nodal principal stresses per element at the shared node ($\sigma_{11,k}$ in Fig. 9b).

Table 5 summarises the nomenclature, where available, used by each FE software to define procedures (a) and (b) for principal stress averaging, according to Fig. 9. The table reports also the *default option* adopted by individual FE codes and it is seen that option (a) is the default for Ansys, Lusas and Solidworks, while option (b) is the default for Abaqus and the post-processor Hyperview.

To investigate the effects of options (a) and (b) on K^{*}_{FE} value to be adopted in Eq. (4), the mode I problems of Figs. 3a-d have been re-analysed with Ansys Mechanical APDL FE code, but now calculating the maximum principal stress $\sigma_{11,peak}$, using either option (a) or (b) of Fig. 9, instead of the opening peak stress $\sigma_{\theta\theta,\theta=0,peak}$. The obtained results are reported in Figs. 9c-f, which show that the mean values of K^{*}_{FE} are all inside the scatter bands previously calibrated using the opening peak stress $\sigma_{\theta\theta,\theta=0,peak}$ (Fig. 4), regardless the procedure adopted for principal stress averaging. However, Figs. 9c-f show

that when using procedure (b), the resulting K^*_{FE} values are on average well below the mean value of K^*_{FE} reported in Fig. 4.

7.3 FE mesh pattern

When analysing a given geometry with the same average element size *d*, the FE software packages generate different FE mesh patterns.
The influence of different FE meshes has been analysed by considering as case study the mode I problem of Fig. 3d, i.e. a full-penetration cruciform welded joint under axial loading, having thickness $2a$ = 13 mm, notch opening angle at the weld toe 2α = 135° and global element size d = 3 mm. The mesh patterns generated by all considered FE codes are reported in Figs. 10a-g. Discrepancies in the mesh patterns can be noted from visual inspectionf Figs. 10a-g; therefore, a more detailed analysis has been performed to allow a quantitative comparison. Figure 10h reports the number of finite elements that share each vertex node belonging to the weld toe line and show that it is highly scattered, being in the range between 6 (at free surface) and 24, and it has a different trend for different mesh patterns. Figure 10i reports the size of finite elements, i.e. the length of the tetrahedron edges, that share each vertex node belonging to the weld toe line. The figure reports the mean size of the elements along with the relevant bar, which represents the range between maximum and minimum sizes evaluated at each node. Figure 10i shows that the average element size closely matches the nominal one for Ansys and Abaqus, while it is always larger for Lusas, LS-dyna and Optistruct and always smaller for Solidworks. Moreover, the element size has a strong variability in the range between $0.55 \cdot d_{nom}$ and $1.85 \cdot d_{nom}$.
The great differences in the mesh patterns highlighted in Figs. 10h and 10i, only slightly affect the peak stress distributions. Indeed, Fig. 10l and Fig. 10m show that the mesh patterns of four-node and ten-node tetra elements provide an opening peak stress in the range 0.944–1.197 MPa and 1.417–1.763 MPa, respectively, when considering FE codes which apply Eq. (11) to extrapolate stresses at nodes. Despite the strong variability of both the number of finite elements sharing a node and the finite element size above mentioned, the effects on the peak stress distribution are reduced and are demonstrated by the relatively reduced deviations of the K_{FE} parameters in the range between ±8% and ±30%.

7.4 Finite element formulation

All FE codes involved in the present Round Robin integrate four-node and ten-node tetra elements by using 1 and 4 Gauss points, respectively, Ansys Mechanical APDL being the only exception since it adopts 4 Gauss points also for the four-node tetra element, as reported in Table 2.
To analyse the effect of different finite element formulations, the 3D mode I problem of the full-penetration cruciform welded joint reported in Fig. 3d has been taken again as a case study. The effect of the FE mesh has been excluded by generating two mesh patterns, one using four-node tetra and the other using ten-node tetra elements, and adopting in both cases the free mesh generation algorithm available in Solidworks with *blend option* activated (see Fig. 10e). Afterwards, the mesh patterns have been imported into all other FE codes to keep identical FE meshes in all analyses.
The obtained results in terms of opening peak stress $\sigma_{\theta\theta,\theta=0,peak}$, evaluated at the vertex nodes belonging to the weld toe line (z-direction in Fig. 10e), are reported in Fig. 11a and b for four-node and ten-node tetra elements, respectively. Figure 11a shows that the peak stress values are perfectly matching for all FE codes, which adopt 1 Gauss point to integrate the four-node tetra element, even for LS-Dyna and Optistruct, since the centroid coincides with the sole Gauss point. On the other hand, Ansys Mechanical APDL, which adopts 4 Gauss points, delivers different results and on average slightly higher than those calculated by the other FE codes. Figure 11b illustrates a perfect match of the ten-node tetra elements available in all FE codes involved in the present Round Robin, with the only exceptions of LS-Dyna and Optistruct, as it was expected since all codes adopt 4 Gauss points. Moreover, Figs. 11b confirms once again that Ansys Mechanical APDL, when Eq. (12) is enforced to extrapolate stresses at FE nodes, provides results coincident with those generated by LS-Dyna and Optistruct, provided that also the mesh pattern and the element formulation are kept the same.

8. CONCLUSIONS

A Round Robin activity has been performed to calibrate the Peak Stress Method (PSM) adopting different FE software packages for a range of coarse FE meshes. The PSM is an engineering, numerical tool, originally calibrated using Ansys Mechanical APDL FE code to evaluate rapidly the mode I, II and III linear elastic Notch Stress Intensity Factors (NSIFs), respectively. To do so, the PSM employs the linear elastic, opening, in-plane shear and out-of-plane shear peak stresses, respectively, evaluated at the sharp V-notch tip. Three non-dimensional parameters are required to apply the PSM, namely K^*_{FE} (Eq. (4)), K^{**}_{FE} (Eq. (5)) and K^{***}_{FE} (Eq. (6), which have been calibrated here adopting four-node and ten-node tetrahedral finite elements available in commercial FE codes, namely Ansys Mechanical APDL, Ansys Mechanical, Abaqus, Lusas, Solidworks, Hypermesh/LS-Dyna/Hyperview and Hypermesh/Optistruct/Hyperview. All in all, 362 3D FE analyses have been performed for each of the 16 different combinations of FE codes and participants, the total number of analyses being 5792. The following conclusions can be drawn:

- The PSM parameters K^{*}_{FE}, K^{**}_{FE} and K^{***}_{FE} and the minimum mesh density ratios a/d to guarantee their convergence within a given scatter, result to be dependent on the FE code, element type, notch opening angle and procedure to calculate stresses at FE nodes.
- The main sources of discrepancy among the PSM parameters calculated with the different FE codes are (i) the different methods adopted to extrapolate stresses at FE nodes according to Eqs (10) or (11); (ii) the different mesh pattern generated, in terms of number of elements sharing a node and actual finite element size for the same input size given by the FE analyst.
- Additional differences among the considered FE software packages, which affects the results to some extent, include (i) the finite element formulation, in terms of number of Gauss points and (ii) the numerical procedure adopted for principal stress averaging at FE nodes, which is relevant in some particular cases illustrated in the paper. However, the effects of such differences are taken up by the scatter bands defined for the PSM parameters.
- 3D mesh patterns being coarse and post-processing the evaluated peak stresses being rather rapid and simple, the 3D PSM based on tetra elements seems useful for engineers involved in structural FE analyses of components weakened by sharp V-shaped notches, even when large-scale and geometrically complex structures are investigated.

APPENDIX A: details of mesh generation settings

Details relevant to element type and settings to generate a free 3D FE mesh are reported in the following for each FE code:

- ***Ansys® Mechanical APDL***
  Element type: Solid → Tet 4-node (SOLID 285) or Tet 10-node (SOLID 187)
  Element options: not applicable
  Element size: Size Cntrls → Manual Size → Global → Size = *d*
  Mesh generation: Mesh → Volumes → Free
- ***Ansys® Mechanical***
  Element type: Tet4 (SOLID 185) or Tet10 (SOLID 187)
  Element options: not applicable
  Element size: Mesh → Insert → Sizing → Type = Element Size → Element Size = *d*
  Mesh generation: Mesh → Insert → Method → Method = Tetrahedrons → Element Order = Linear (for Tet4) or Quadratic (for Tet10); Mesh → Sizing → Use Adaptive Sizing = No → Mesh Defeaturing = No; Mesh → Generate Mesh
- ***Dassault Systèmes® Abaqus***
  Element type: Quad
  Element options: Plane strain, Incompatible modes (CPE4I)
  Element size: Global Seeds → Sizing Cntrls → Approximate global size = *d*
  Mesh generation: Mesh Cntrls → Free → Advancing front → "Use mapped meshing where appropriate" MUST BE INACTIVE; Mesh Part Instance → Ok
- ***Lusas®***
  Element type: 3D isoparametric tetrahedra solid continuum element with higher order models capable of modelling curved boundaries (TH4)
  Element options: 4 (TH4) or 10 (TH10) nodes
  Element size: Mesh → Volume Mesh → Irregular mesh → Element size = d
  Mesh generation: Mesh → Volume Mesh
- ***Dassault Systèmes® Solidworks***
  Element type: First-order tetrahedral (Draft quality) or Second-order tetrahedral (High quality)
  Element options: not applicable
  Element Size and Mesh generation: Mesh → Create Mesh → Definition → Mesh Parameters: Blended curvature-based mesh; Maximum element size = Minimum element size = *d*; Mesh Quality → Specify: Draft or High → OK
- ***Altair® Hypermesh/LS-Dyna/Hyperview***
  Element type: Tetra 4 nodes Elform 10, tetra 10 nodes Elform 17 (*LS-Dyna*)
  Element options: not applicable
  Element size: 2D → Automesh → Surfs → Size and bias → Element size = d (*Hypermesh*)
  Mesh generation: 2D → Automesh → Surfs → Size and bias → Mesh type → trias; mesh → 3D → Tetramesh → Tetra mesh → Fixed trias/quads to tetra mesh; mesh (*Hypermesh*)
- ***Altair® Hypermesh/Optistruct/Hyperview***
  Element type: Shell 4-node (*Hypermesh*)
  Element options: Element formulation 13 (Plane strain x-y plane) (*Optistruct*)

Element size: Mesh → Surfs → Size and bias → Element size = d *(Hypermesh)*
Mesh generation: Mesh → Surfs → Mesh type → quads; mesh (*Hypermesh*)

ACKNOWLEDGEMENTS

The Round Robin was conceived and conducted by the Working Group on "*Joining Techniques*" of the Italian Scientific Association for Stress Analysis (AIAS). The precious effort of all participants is gratefully acknowledged.

REFERENCES

1. Eurocode 3 . (2005). Eurocode 3: Design of steel structures – part 1–9: Fatigue. CEN.
2. Hobbacher AF (2016). *Recommendations for Fatigue Design of Welded Joints and Components*. IIW Collection. Springer International Publishing. Epub ahead of print 2016. DOI: 10.1007/978-3-319-23757-2.
3. Fricke W (2003). Fatigue analysis of welded joints: state of development. *Mar. Struct.*, 16, 185–200.
4. Bruder T, Störzel K, Baumgartner J, Hanselka H (2012). Evaluation of nominal and local stress based approaches for the fatigue assessment of seam welds. *Int. J. Fatigue*, 34, 86–102.
5. Poutiainen I, Marquis G (2006). A fatigue assessment method based on weld stress. *Int. J. Fatigue*, 28, 1037–1046.
6. Poutiainen I, Tanskanen P, Marquis G (2004). Finite element methods for structural hot spot stress determination—a comparison of procedures. *Int. J. Fatigue*, 26, 1147–1157.
7. Niemi E, Fricke W, Maddox SJ (2018). *Structural Hot-Spot Stress Approach to Fatigue Analysis of Welded Components - Designer's Guide*. Singapore: Springer Singapore. Epub ahead of print 2018. DOI: 10.1007/978-981-10-5568-3.
8. Yıldırım HC (2014). Fatigue strength assessment of HFMI-treated butt welds by the effective notch stress method. *Weld. World*, 58, 279–288.
9. Leitner M, Simunek D, Shah SF, Stoschka M (2018). Numerical fatigue assessment of welded and HFMI-treated joints by notch stress/strain and fracture mechanical approaches. *Adv. Eng. Softw.*, 120, 96–106.
10. Baumgartner J (2017). Review and considerations on the fatigue assessment of welded joints using reference radii. *Int. J. Fatigue*, 101, 459–468.
11. Baumgartner J, Schmidt H, Ince E, Melz T, Dilger K (2015). Fatigue assessment of welded joints using stress averaging and critical distance approaches. *Weld. World*, 59, 731–742.
12. Radaj D, Sonsino CM, Fricke W (2006). *Fatigue Assessment of Welded Joints by Local Approaches*. 2nd ed. Cambridge: Woodhead Publishing.
13. Fricke W (2012). *IIW recommendations for the fatigue assessment of welded structures by notch stress analysis : IIW-2006-09*. Woodhead Pubhttps://www.sciencedirect.com/book/9780857098559/iiw-recommendations-for-the-fatigue-assessment-of-welded-structures-by-notch-stress-analysis (2012, accessed 22 August 2018).
14. Leitner M, Stoschka M, Ottersböck M (2017). Fatigue assessment of welded and high frequency mechanical impact (HFMI) treated joints by master notch stress approach. *Int. J. Fatigue*, 101, 232–243.
15. Remes H, Gallo P, Jelovica J, Romanoff J, Lehto P (2020). Fatigue strength modelling of high-performing welded joints. *Int. J. Fatigue*, 135, 105555.
16. Shams E, Vormwald M (2017). Fatigue of weld ends under combined loading. *Int. J. Fatigue*, 100, 627–638.
17. Shams E, Malikoutsakis M, Savaidis G, Vormwald M (2014). Notch stress and fracture mechanics based assessment of fatigue of seam weld ends under shear loading. *Fatigue Fract. Eng. Mater. Struct.*, 37, 740–750.
18. Zerbst U, Madia M, Vormwald M (2019). Applying fracture mechanics to fatigue strength determination – Some basic considerations. *Int. J. Fatigue*, 126, 188–201.
19. Nykanen T, Marquis G, Bjork T (2009). A simplified fatigue assessment method for high quality welded cruciform joints. *Int. J. Fatigue*, 31, 79–87.
20. Mikkola E, Murakami Y, Marquis G (2015). Equivalent crack approach for fatigue life assessment of welded joints. *Eng. Fract. Mech.*, 149, 144–155.
21. Sonsino C (1995). Multiaxial fatigue of welded joints under in-phase and out-of-phase local strains and stresses. *Int. J. Fatigue*, 17, 55–70.
22. Susmel L (2009). *Multiaxial notch fatigue*. Cambridge, UK: Woodhead Publishing.
23. Radaj D, Vormwald M (2013). *Advanced Methods of Fatigue Assessment*. Berlin, Heidelberg: Springer Berlin Heidelberg. Epub ahead of print 2013. DOI: 10.1007/978-3-642-30740-9.
24. Lazzarin P, Tovo R (1998). A notch intensity factor approach to the stress analysis of welds. *Fatigue Fract. Eng. Mater. Struct.*, 21, 1089–1103.
25. Lazzarin P, Sonsino CM, Zambardi R (2004). A notch stress intensity approach to assess the multiaxial fatigue

strength of welded tube-to-flange joints subjected to combined loadings. *Fatigue Fract. Eng. Mater. Struct.*, 27, 127–140.
26. Fischer C, Fricke W, Rizzo CM (2016). Experiences and recommendations for numerical analyses of notch stress intensity factor and averaged strain energy density. *Eng. Fract. Mech.*, 165, 98–113.
27. Fischer C, Fricke W, Rizzo CM (2016). Review of the fatigue strength of welded joints based on the notch stress intensity factor and SED approaches. *Int. J. Fatigue*, 84, 59–66.
28. Livieri P, Lazzarin P (2005). Fatigue strength of steel and aluminium welded joints based on generalised stress intensity factors and local strain energy values. *Int. J. Fract.*, 133, 247–276.
29. Lazzarin P, Livieri P, Berto F, Zappalorto M (2008). Local strain energy density and fatigue strength of welded joints under uniaxial and multiaxial loading. *Eng. Fract. Mech.*, 75, 1875–1889.
30. Carpinteri A, Spagnoli A, Vantadori S (2009). Multiaxial fatigue life estimation in welded joints using the critical plane approach. *Int. J. Fatigue*, 31, 188–196.
31. Susmel L (2008). Modified Wöhler curve method, theory of critical distances and Eurocode 3: A novel engineering procedure to predict the lifetime of steel welded joints subjected to both uniaxial and multiaxial fatigue loading. *Int. J. Fatigue*, 30, 888–907.
32. Susmel L (2009). The Modified Wöhler Curve Method calibrated by using standard fatigue curves and applied in conjunction with the Theory of Critical Distances to estimate fatigue lifetime of aluminium weldments. *Int. J. Fatigue*, 31, 197–212.
33. Williams ML (1952). Stress singularities resulting from various boundary conditions in angular corners of plates in tension. *J Appl Mech*, 19, 526–528.
34. Qian J, Hasebe N (1997). Property of eigenvalues and eigenfunctions for an interface V-notch in antiplane elasticity. *Eng. Fract. Mech.*, 56, 729–734.
35. Gross B, Mendelson A (1972). Plane elastostatic analysis of V-notched plates. *Int. J. Fract. Mech.*, 8, 267–276.
36. Lazzarin P, Tovo R (1996). A unified approach to the evaluation of linear elastic stress fields in the neighborhood of cracks and notches. *Int. J. Fract.*, 78, 3–19.
37. Verreman Y, Nie B (1996). Early development of fatigue cracking at manual fillet welds. *Fatigue Fract. Eng. Mater. Struct.*, 19, 669–681.
38. Atzori B, Meneghetti G (2001). Fatigue strength of fillet welded structural steels: finite elements, strain gauges and reality. *Int. J. Fatigue*, 23, 713–721.
39. Lazzarin P, Lassen T, Livieri P (2003). A notch stress intensity approach applied to fatigue life predictions of welded joints with different local toe geometry. *Fatigue Fract. Eng. Mater. Struct.*, 26, 49–58.
40. Nisitani H, Teranishi T (2004). KI of a circumferential crack emanating from an ellipsoidal cavity obtained by the crack tip stress method in FEM. *Eng. Fract. Mech.*, 71, 579–585.
41. Meneghetti G, Lazzarin P (2007). Significance of the elastic peak stress evaluated by FE analyses at the point of singularity of sharp V-notched components. *Fatigue Fract. Eng. Mater. Struct.*, 30, 95–106.
42. Meneghetti G, Guzzella C (2014). The peak stress method to estimate the mode I notch stress intensity factor in welded joints using three-dimensional finite element models. *Eng. Fract. Mech.*, 115, 154–171.
43. Meneghetti G (2012). The use of peak stresses for fatigue strength assessments of welded lap joints and cover plates with toe and root failures. *Eng. Fract. Mech.*, 89, 40–51.
44. Meneghetti G (2013). The peak stress method for fatigue strength assessment of tube-to-flange welded joints under torsion loading. *Weld. World*, 57, 265–275.
45. Meneghetti G, Campagnolo A, Avalle M, Castagnetti D, Colussi M, Corigliano P, De Agostinis M, Dragoni E, Fontanari V, Frendo F, Goglio L, Marannano G, Marulo G, Moroni F, Pantano A, et al. (2018). Rapid evaluation of notch stress intensity factors using the peak stress method: Comparison of commercial finite element codes for a range of mesh patterns. *Fatigue Fract. Eng. Mater. Struct.*, 41,. Epub ahead of print 2018. DOI: 10.1111/ffe.12751.
46. Campagnolo A, Meneghetti G (2018). Rapid estimation of notch stress intensity factors in 3D large-scale welded structures using the peak stress method. *MATEC Web Conf.*, 165,. Epub ahead of print 25 May 2018. DOI: 10.1051/matecconf/201816517004.
47. Campagnolo A, Roveda I, Meneghetti G (2019). The Peak Stress Method combined with 3D finite element models to assess the fatigue strength of complex welded structures. *Procedia Struct. Integr.*, 19, 617–626.
48. Meneghetti G, Lazzarin P (2011). The Peak Stress Method for Fatigue Strength Assessment of welded joints with weld toe or weld root failures. *Weld. World*, 55, 22–29.
49. Meneghetti G, Campagnolo A, Rigon D (2017). Multiaxial fatigue strength assessment of welded joints using the Peak Stress Method – Part I: Approach and application to aluminium joints. *Int. J. Fatigue*, 101, 328–342.
50. Meneghetti G, Campagnolo A, Rigon D (2017). Multiaxial fatigue strength assessment of welded joints using the Peak Stress Method – Part II: Application to structural steel joints. *Int. J. Fatigue*, 101, 343–362.
51. Radaj D (2014). State-of-the-art review on extended stress intensity factor concepts. *Fatigue Fract. Eng. Mater. Struct.*, 37, 1–28.

52. Radaj D (2015). State-of-the-art review on the local strain energy density concept and its relation to the J -integral and peak stress method. *Fatigue Fract. Eng. Mater. Struct.*, 38, 2–28.
53. Berto F, Lazzarin P (2014). Recent developments in brittle and quasi-brittle failure assessment of engineering materials by means of local approaches. *Mater. Sci. Eng. R Reports*, 75, 1–48.
54. Meneghetti G, Campagnolo A (2020). State-of-the-art review of peak stress method for fatigue strength assessment of welded joints. *Int. J. Fatigue*, 139, 105705.
55. Campagnolo A, Ferro P, Romanin L, Meneghetti G (2021). Residual notch stress intensity factors in welded joints evaluated by 3D numerical simulations of arc welding processes. *Materials (Basel).*, 14,. Epub ahead of print 2021. DOI: 10.3390/ma14040812.
56. Zienkiewicz OC, Taylor RL, Zhu JZ (2013). *The Finite Element Method: its Basis and Fundamentals*. Elsevier. Epub ahead of print 2013. DOI: 10.1016/C2009-0-24909-9.
57. Bathe KJ (1995). *Finite Element Procedures*. Pearson College Div.

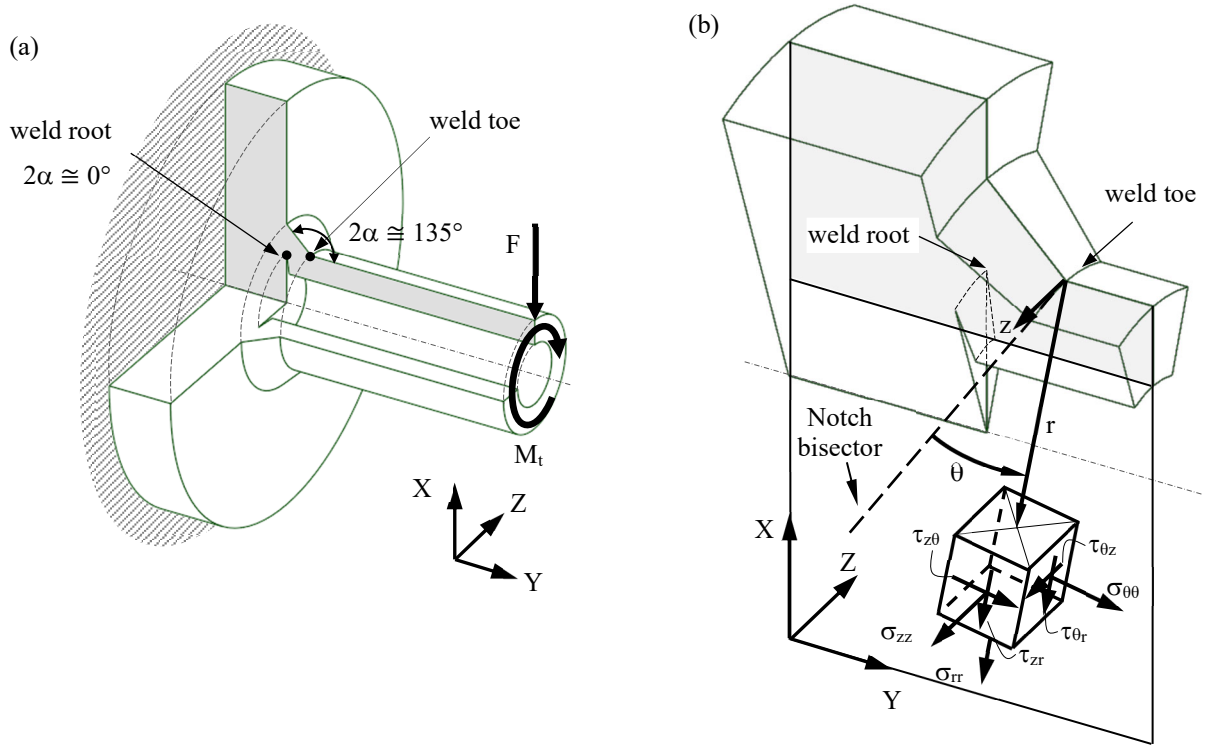

Figure 1: (a) Partial-penetration tube-to-flange welded joint under combined bending and torsion fatigue loading. The sharp V-notch opening angle 2α is typically 0° at the weld root and 135° at the weld toe. (b) Cylindrical reference system (r,θ,z) centred at the weld toe and singular stress components. See also Ref. [54].

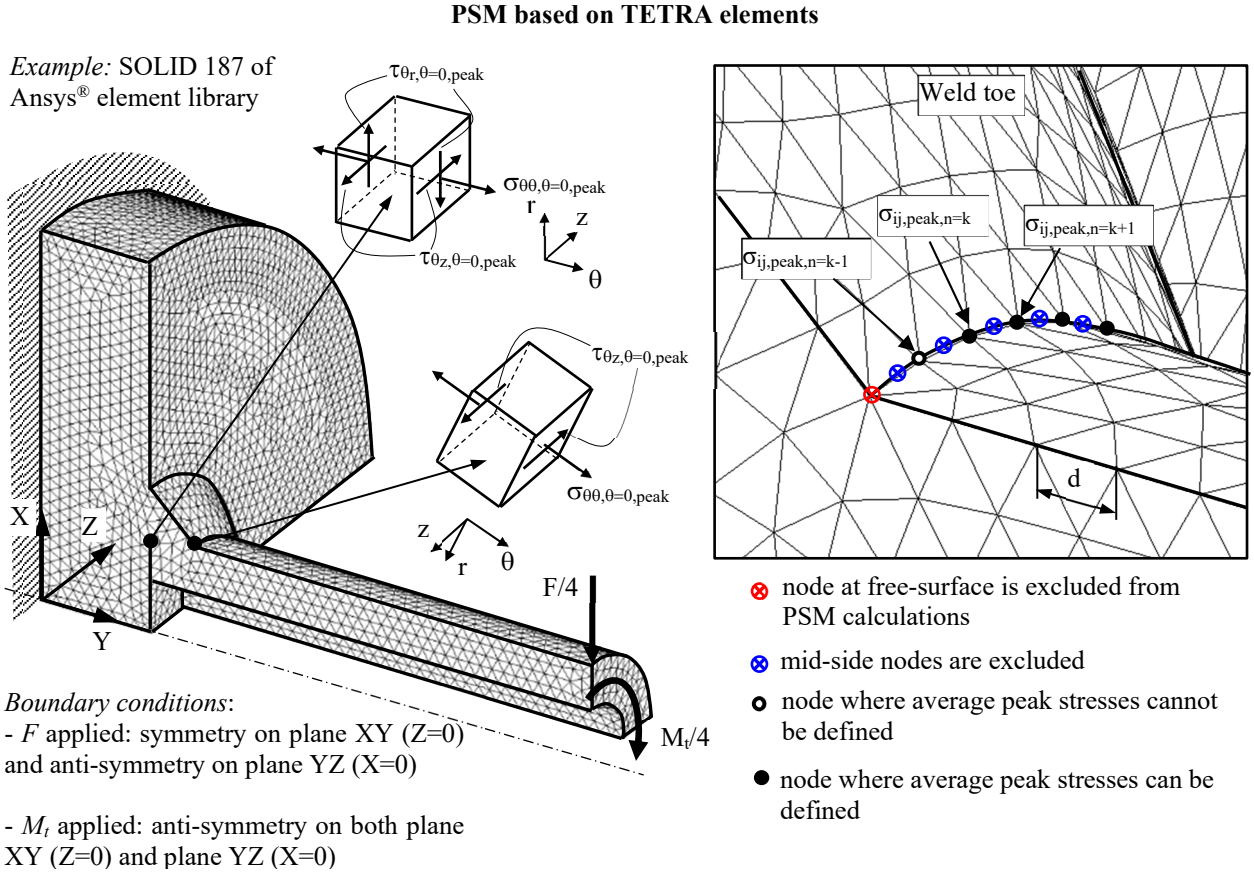

Figure 2: FE model to apply the PSM according to Eqs. (4)-(6) to a partial-penetration tube-to-flange welded joint under combined bending and torsion loading using ten-node tetra elements. See also Ref. [54].

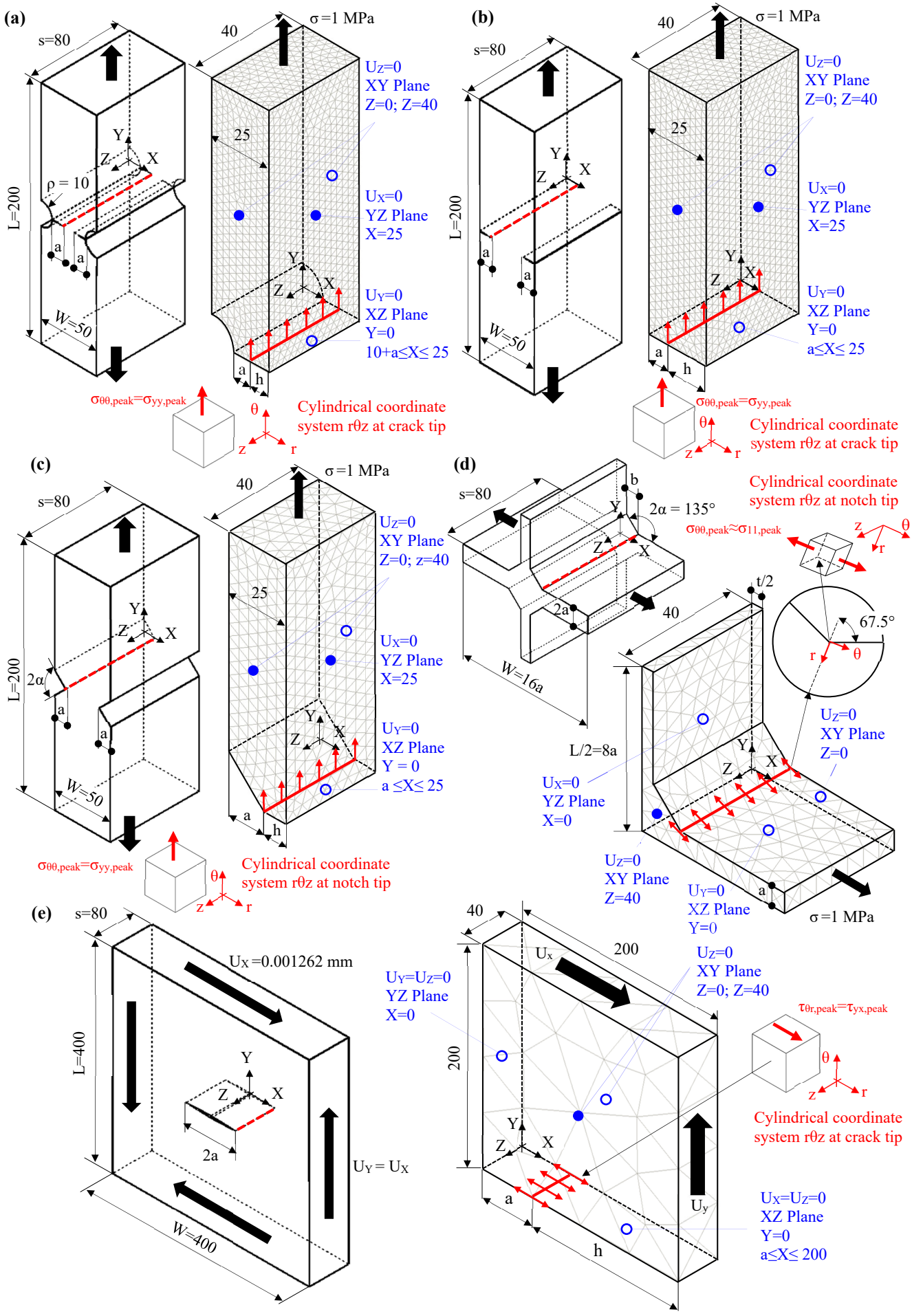
(a)
s=80
40
σ=1 MPa
L=200
ρ = 10
a
a
W=50
25
Y
Z
X
U_Z=0
XY Plane
Z=0; Z=40
U_X=0
YZ Plane
X=25
U_Y=0
XZ Plane
Y=0
10+a≤X≤ 25
h
$\sigma_{\theta\theta,peak}=\sigma_{yy,peak}$
θ
z
r
Cylindrical coordinate
system rθz at crack tip
(b)
s=80
40
σ=1 MPa
L=200
a
W=50
25
U_Z=0
XY Plane
Z=0; Z=40
U_X=0
YZ Plane
X=25
U_Y=0
XZ Plane
Y=0
a≤X≤ 25
h
$\sigma_{\theta\theta,peak}=\sigma_{yy,peak}$
Cylindrical coordinate
system rθz at crack tip
(c)
s=80
40
σ=1 MPa
L=200
2α
a
a
W=50
25
U_Z=0
XY Plane
Z=0; z=40
U_X=0
YZ Plane
X=25
U_Y=0
XZ Plane
Y = 0
a ≤X≤ 25
h
$\sigma_{\theta\theta,peak}=\sigma_{yy,peak}$
Cylindrical coordinate
system rθz at notch tip
(d)
s=80
b
2α = 135°
2a
W=16a
40
t/2
67.5°
L/2=8a
U_X=0
YZ Plane
X=0
U_Z=0
XY Plane
Z=0
U_Z=0
XY Plane
Z=40
U_Y=0
XZ Plane
Y=0
a
σ=1 MPa
$\sigma_{\theta\theta,peak}\approx\sigma_{11,peak}$
Cylindrical coordinate
system rθz at notch tip
(e)
s=80
U_X =0.001262 mm
L=400
2a
W=400
$U_Y = U_X$
40
200
U_X
$U_Y=U_Z$=0
YZ Plane
X=0
U_Z=0
XY Plane
Z=0; Z=40
200
U_y
$U_X=U_Z$=0
XZ Plane
Y=0
a≤X≤ 200
h
a
$\tau_{\theta r,peak}=\tau_{yx,peak}$
Cylindrical coordinate
system rθz at crack tip

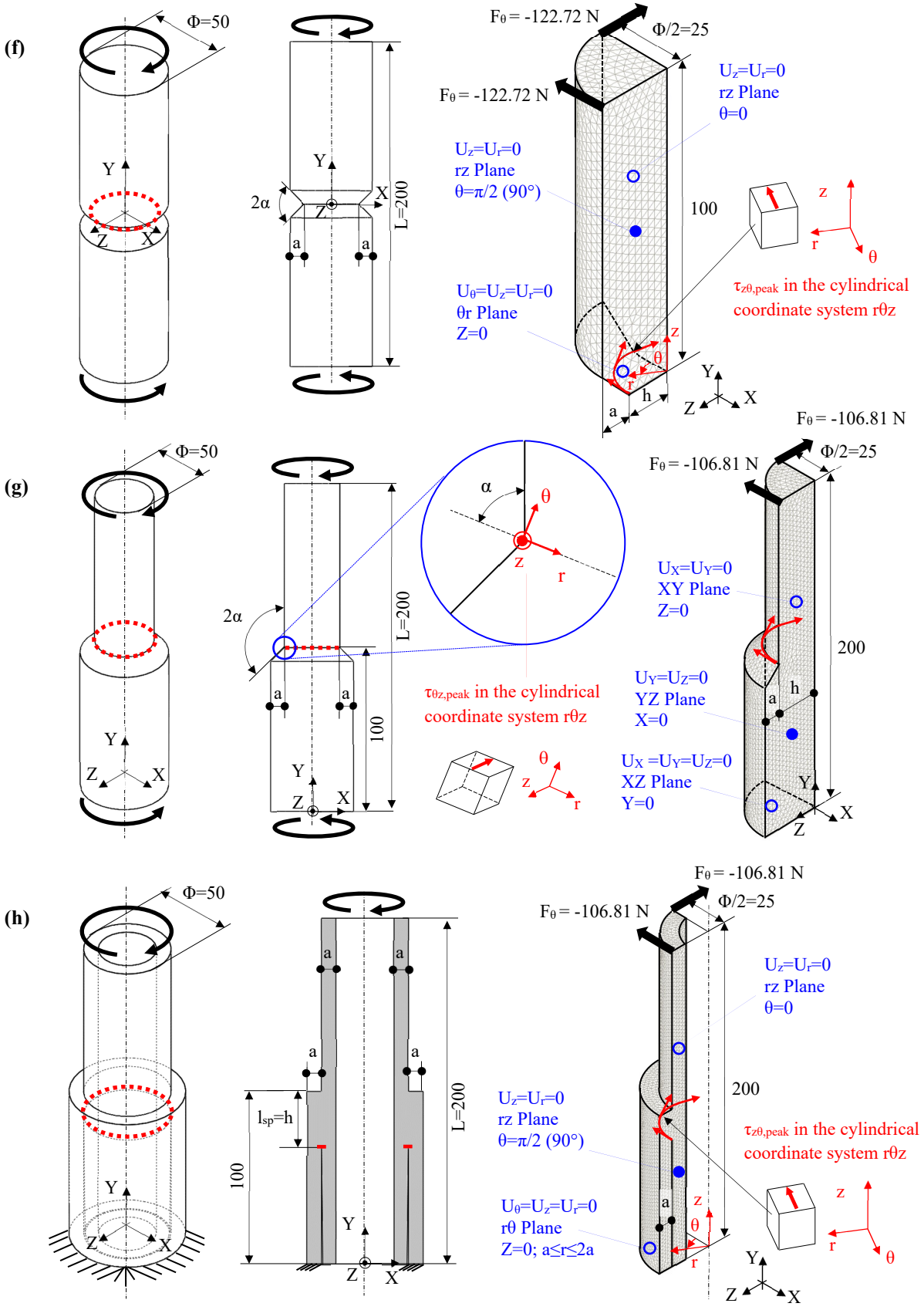

Figure 3: Geometries of 3D problems under mode I (a)-(d), mode II (e) and mode III (f)-(h) loadings analysed according to the PSM. FE mesh patterns of tetra elements, generated by using Ansys® Mechanical APDL, and boundary conditions applied to the FE models. Dimensions are in [mm].

MODE I

FE CODE	TETRA 4 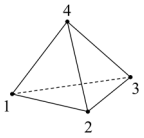	TETRA 10 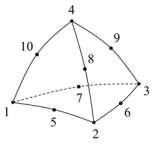
Ansys® Mechanical APDL	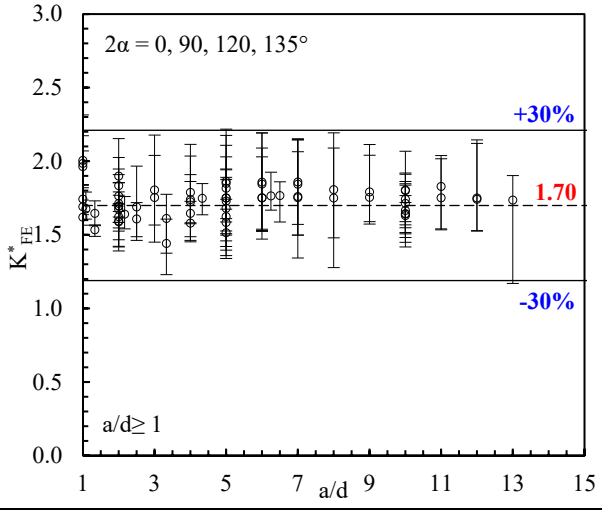	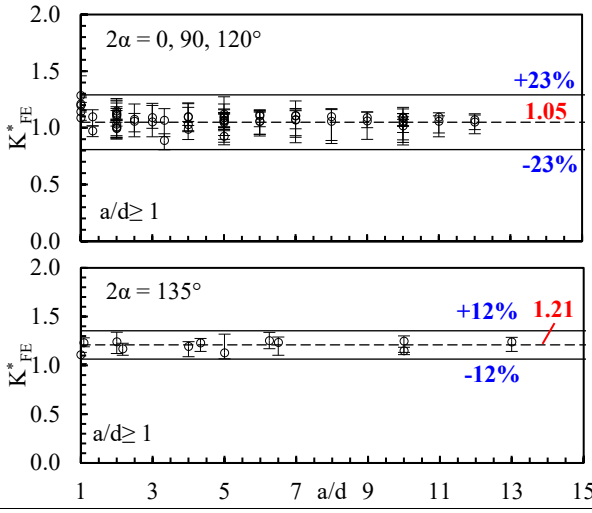
Ansys® Mechanical	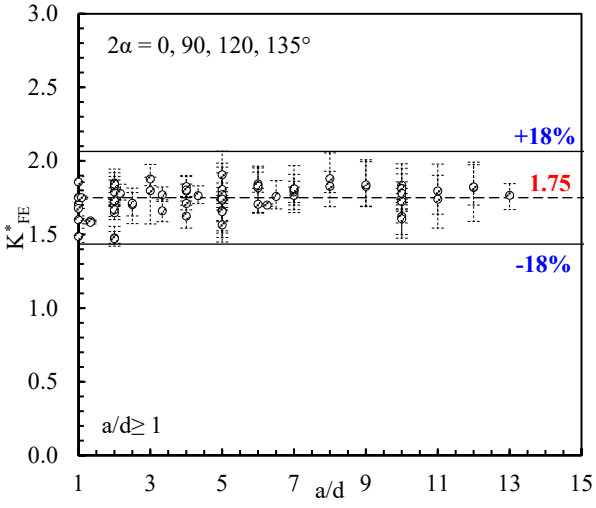	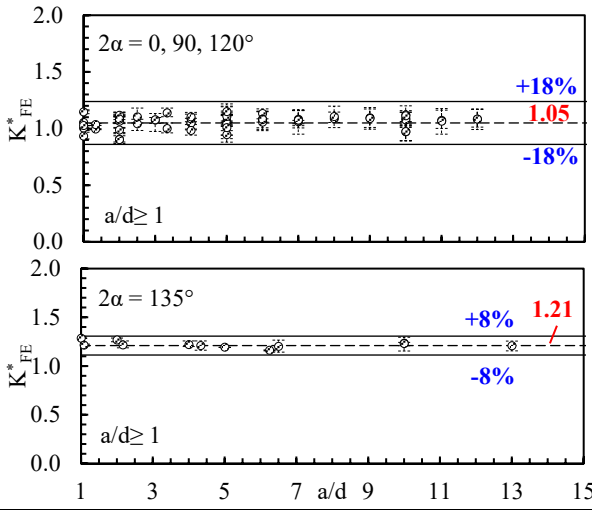
Dassault Systèmes® Abaqus	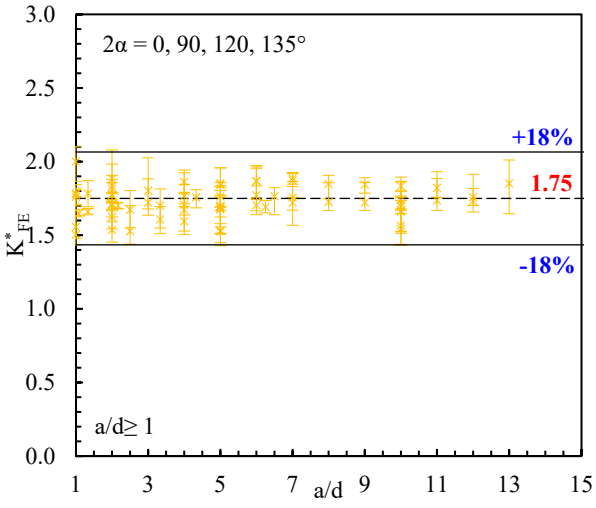	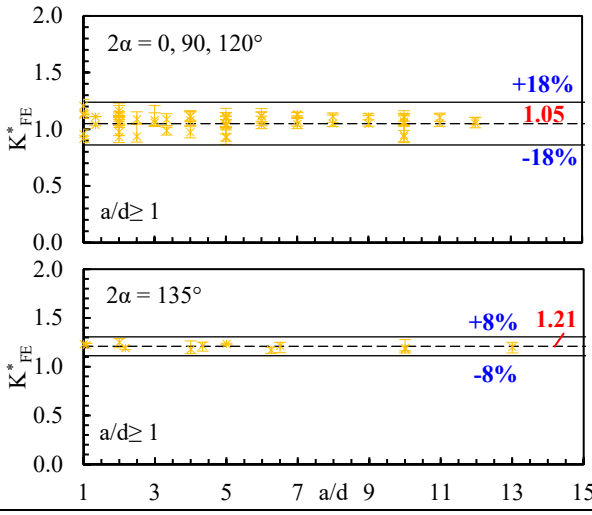

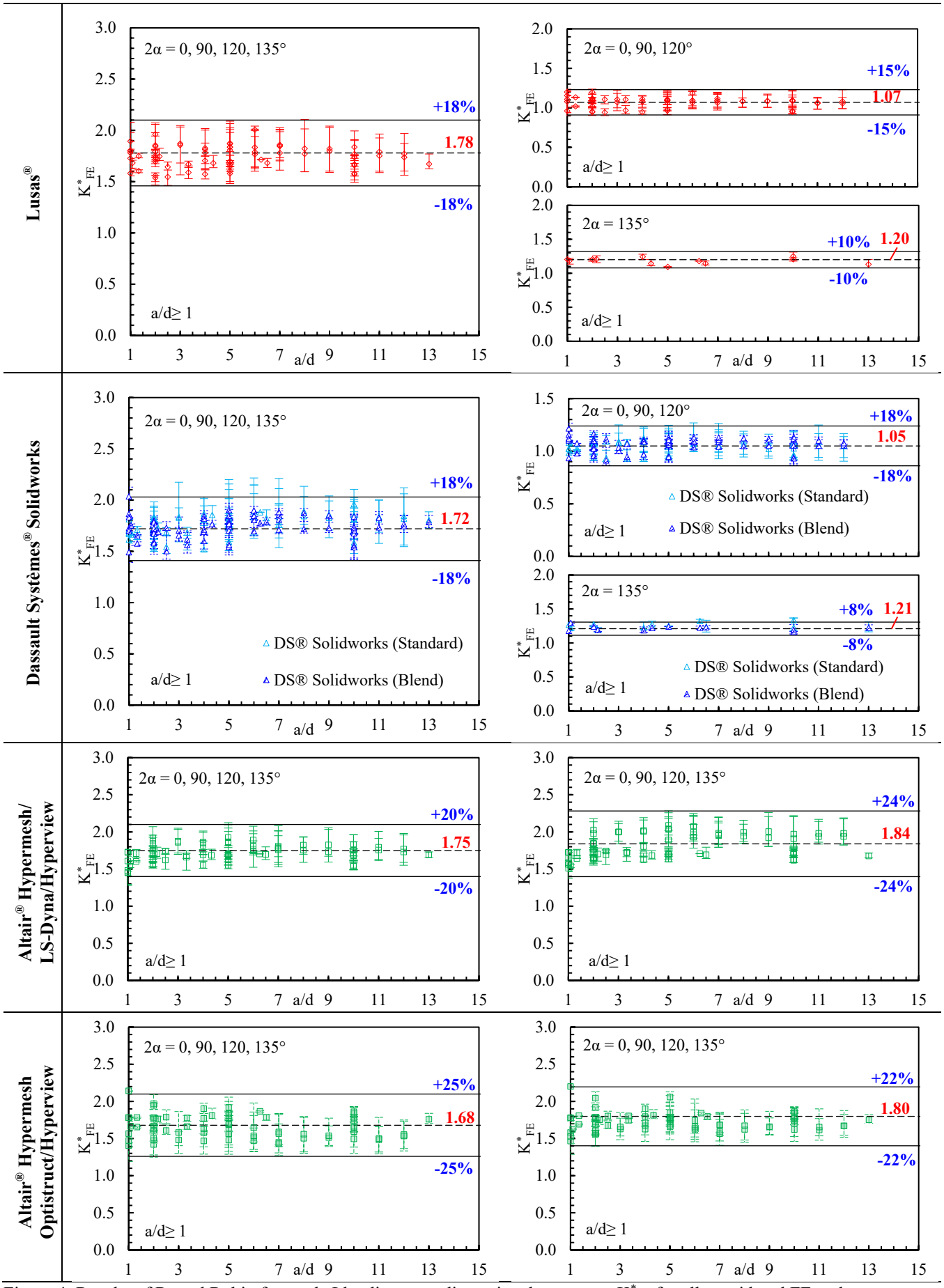

Figure 4: Results of Round Robin for mode I loading: non-dimensional parameter K^*_{FE} for all considered FE codes.

MODE II

FE CODE	TETRA 4 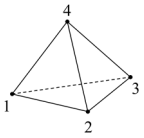	TETRA 10 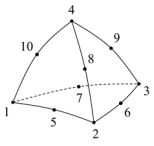
Ansys® Mechanical APDL	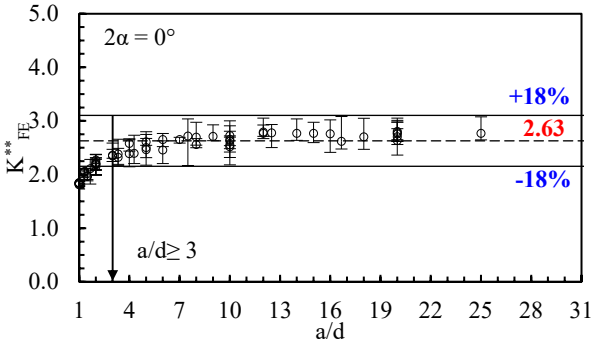	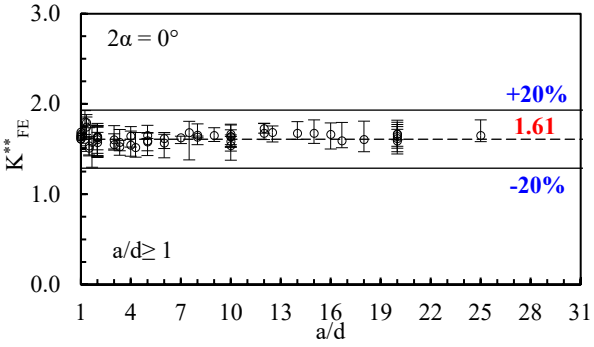
Ansys® Mechanical	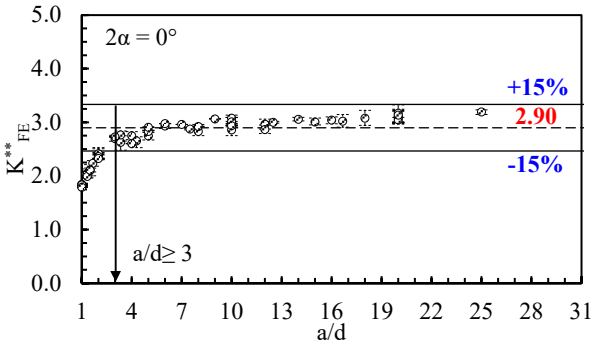	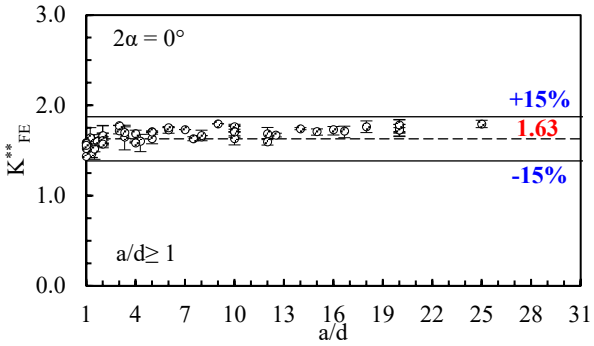
Dassault Systèmes® Abaqus	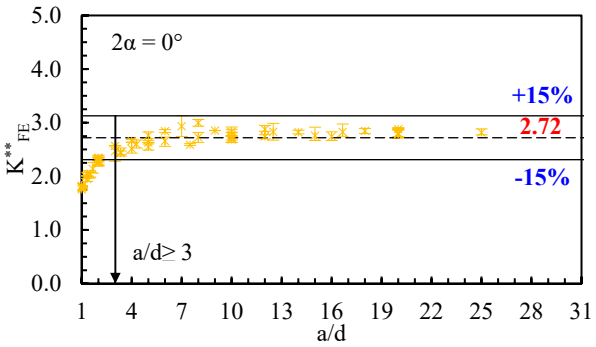	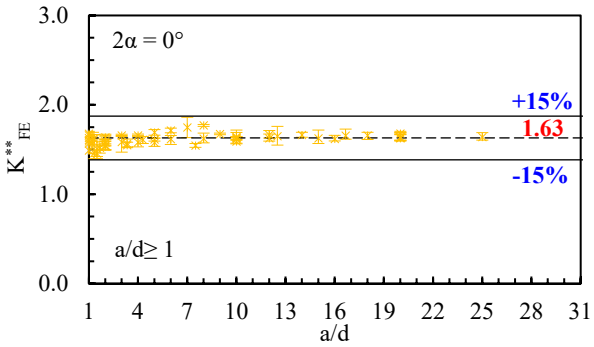
Lusas®	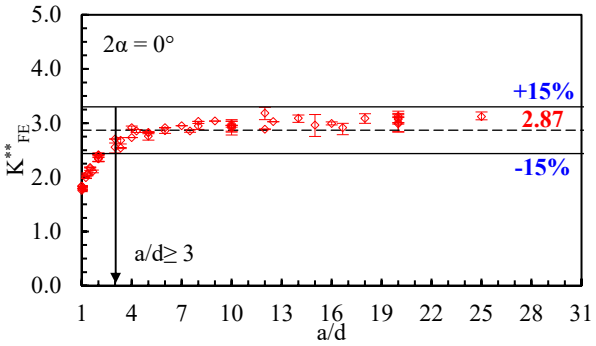	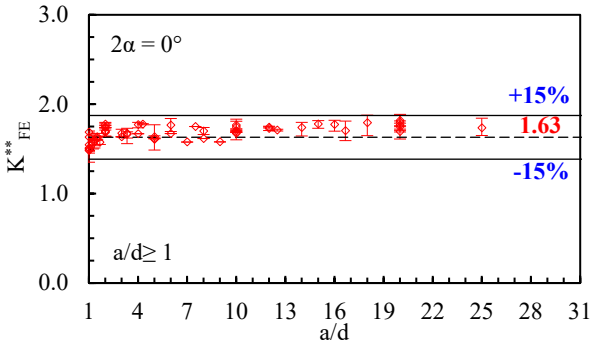

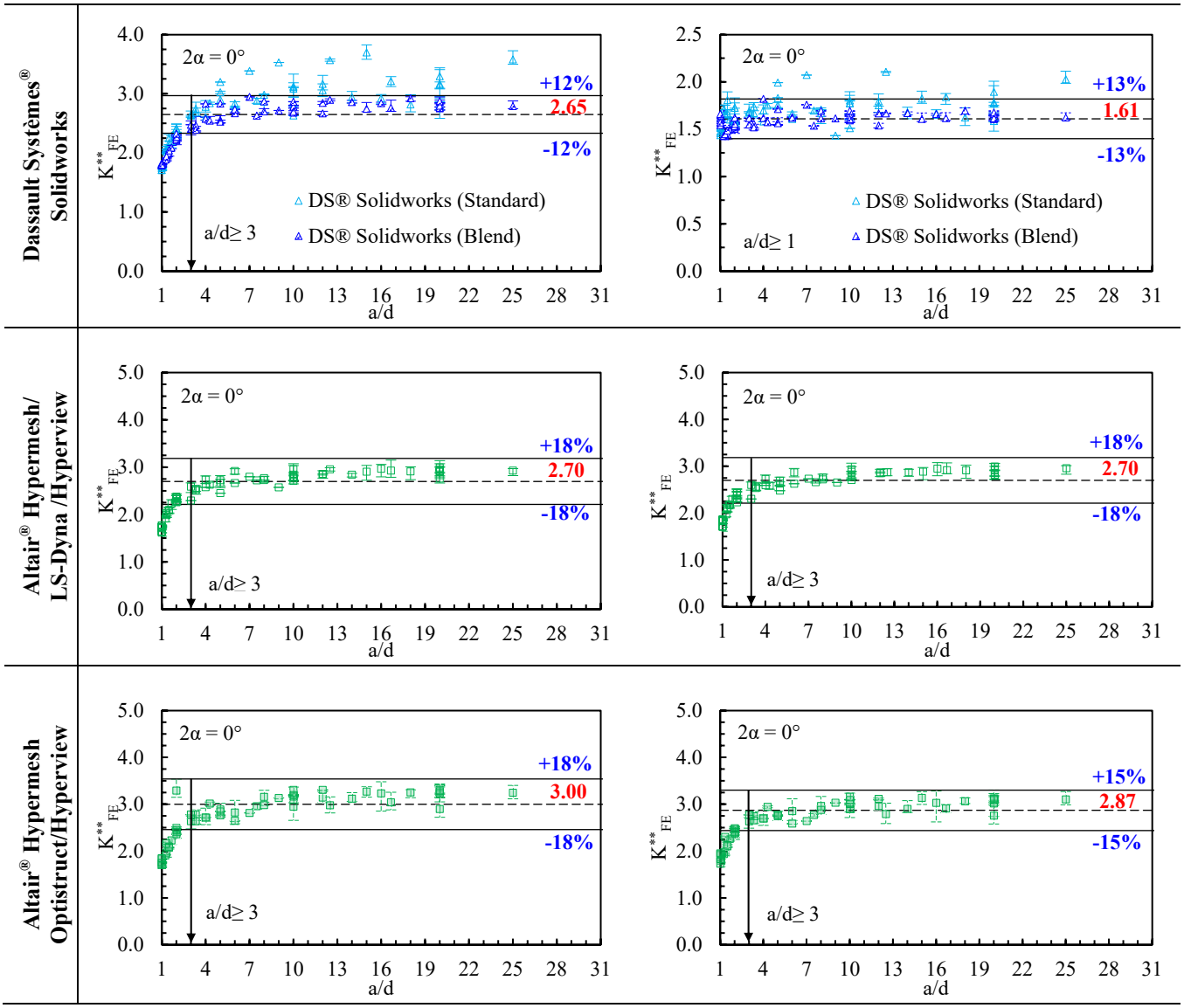

Figure 5: Results of Round Robin for mode II loading: non-dimensional parameter K^{**}_{FE} for all considered FE codes.

MODE III

FE CODE	TETRA 4	TETRA 10
Ansys® Mechanical APDL	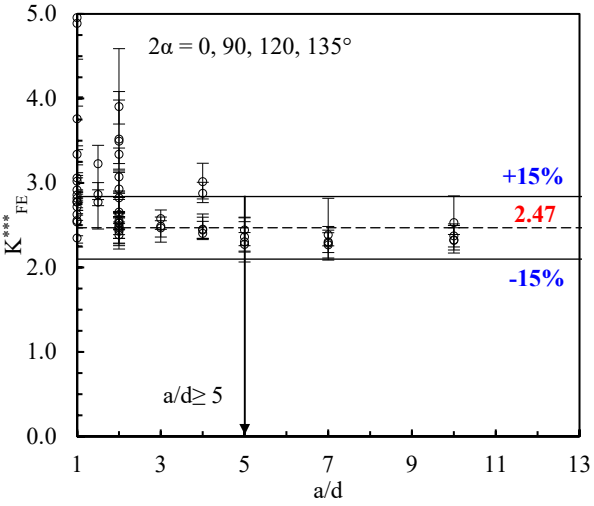	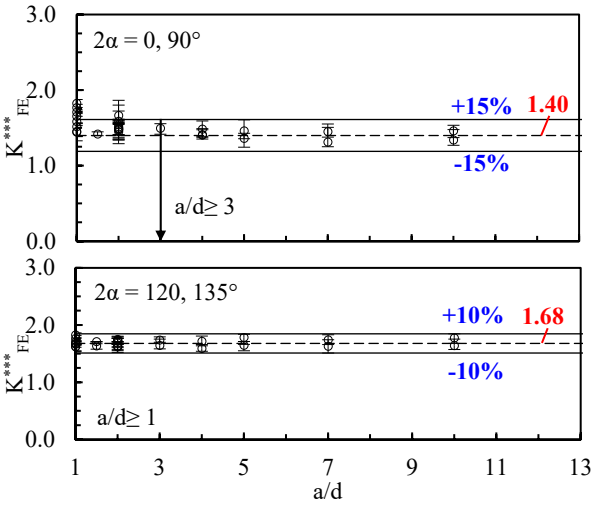
Ansys® Mechanical	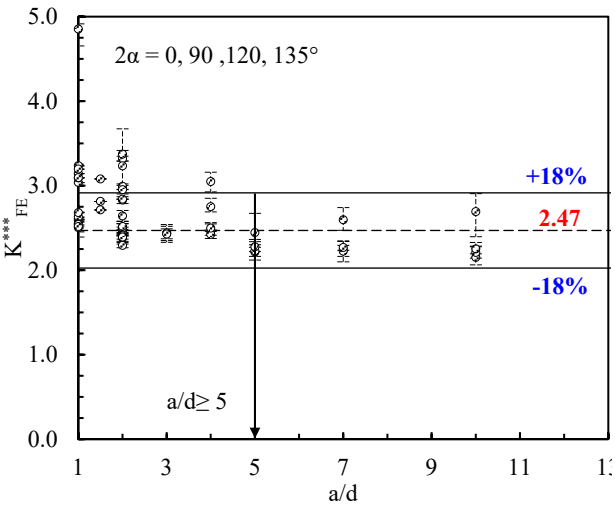	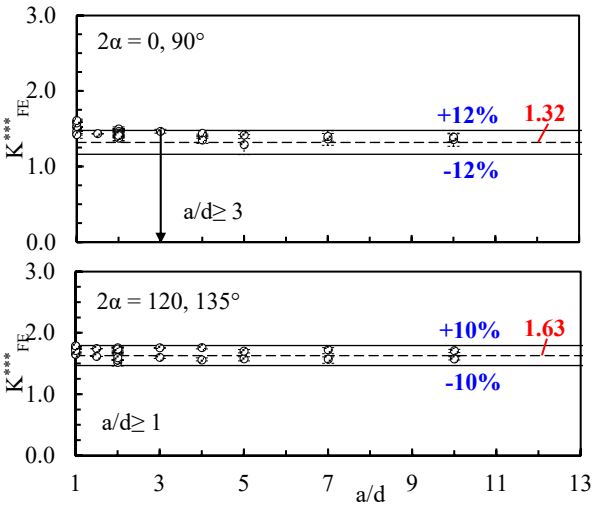
Dassault Systèmes® Abaqus	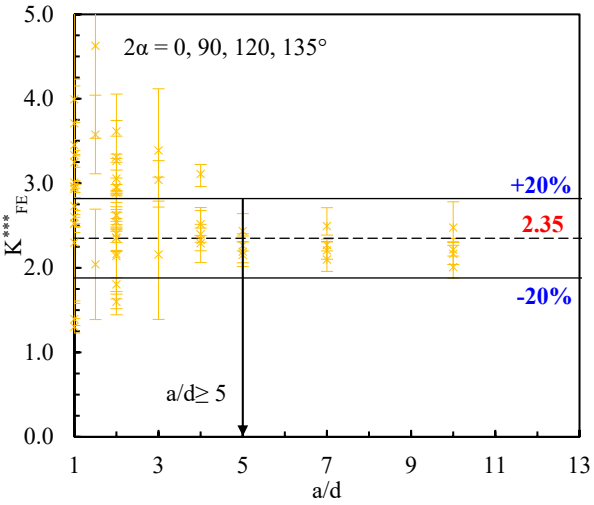	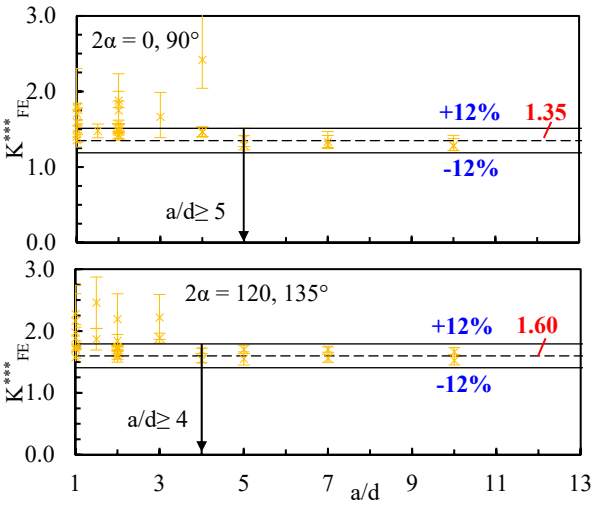

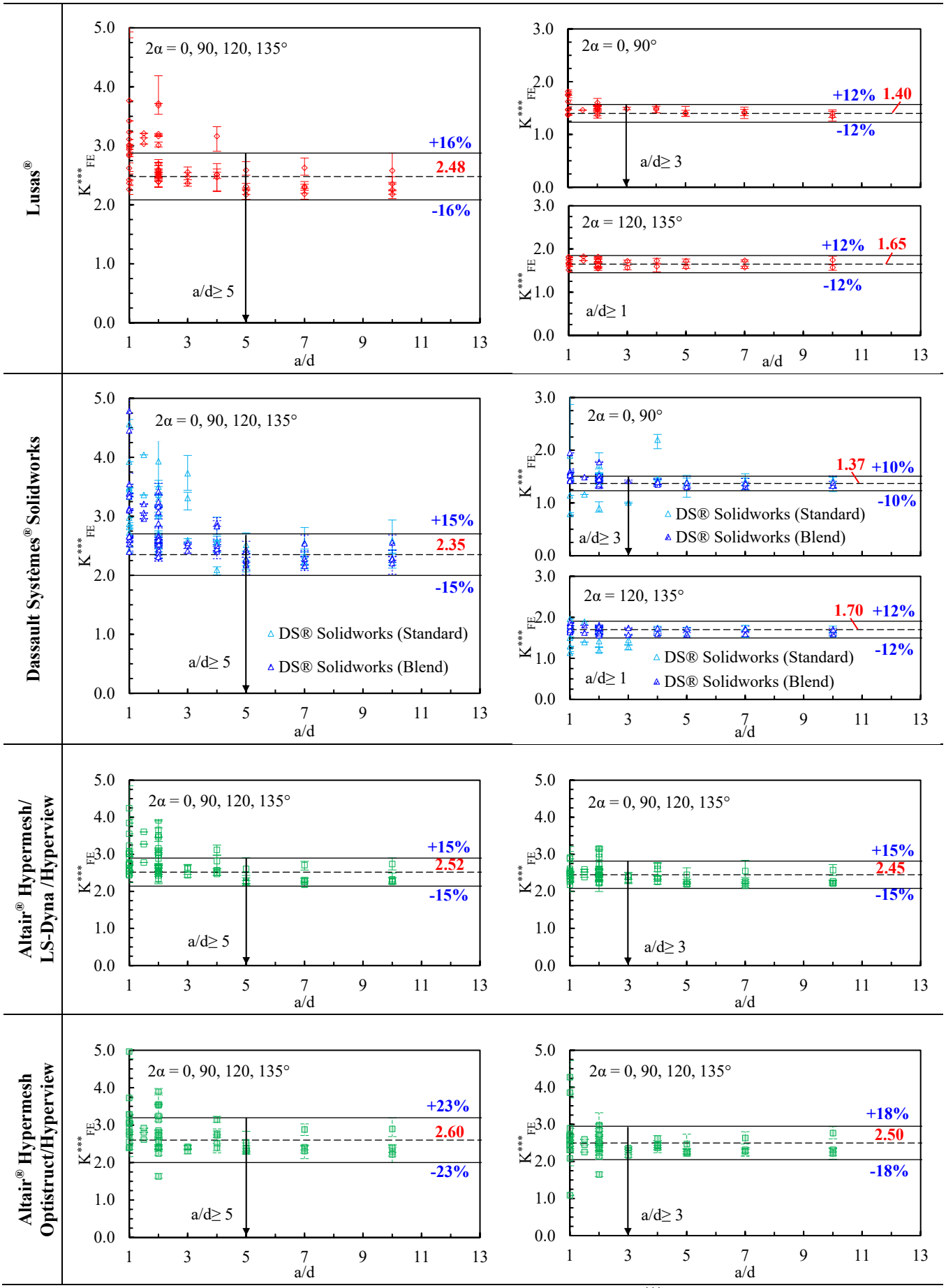

Figure 6: Results of Round Robin for mode III loading: non-dimensional parameter K^{***}_{FE} for all considered FE codes.

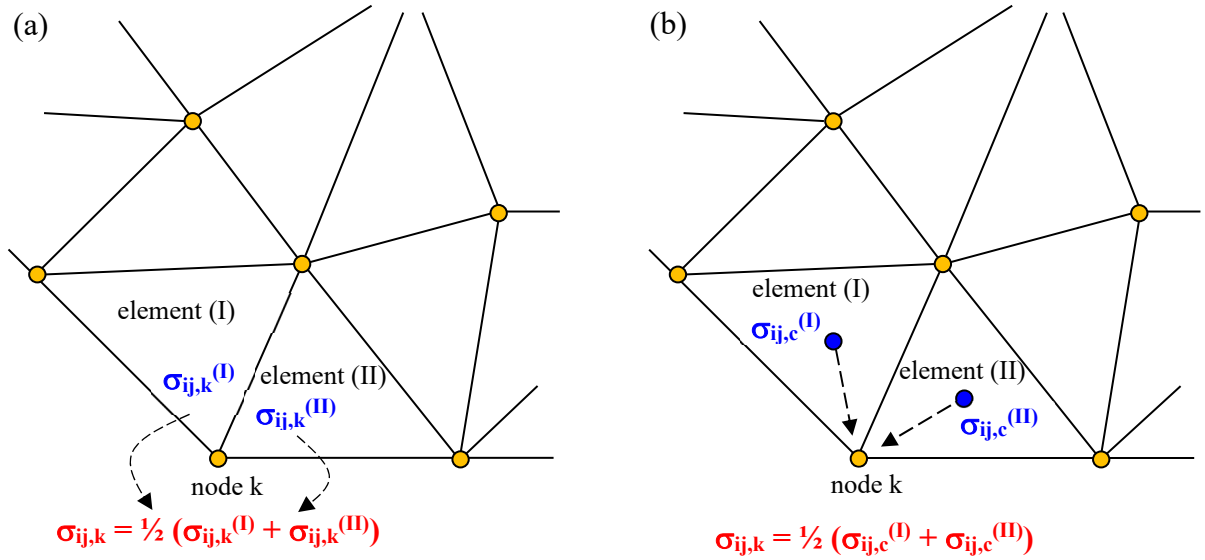

Figure 7: Stress extrapolation at FE nodes based on (a) nodal stresses or (b) centroidal stresses. See also Ref. [45].

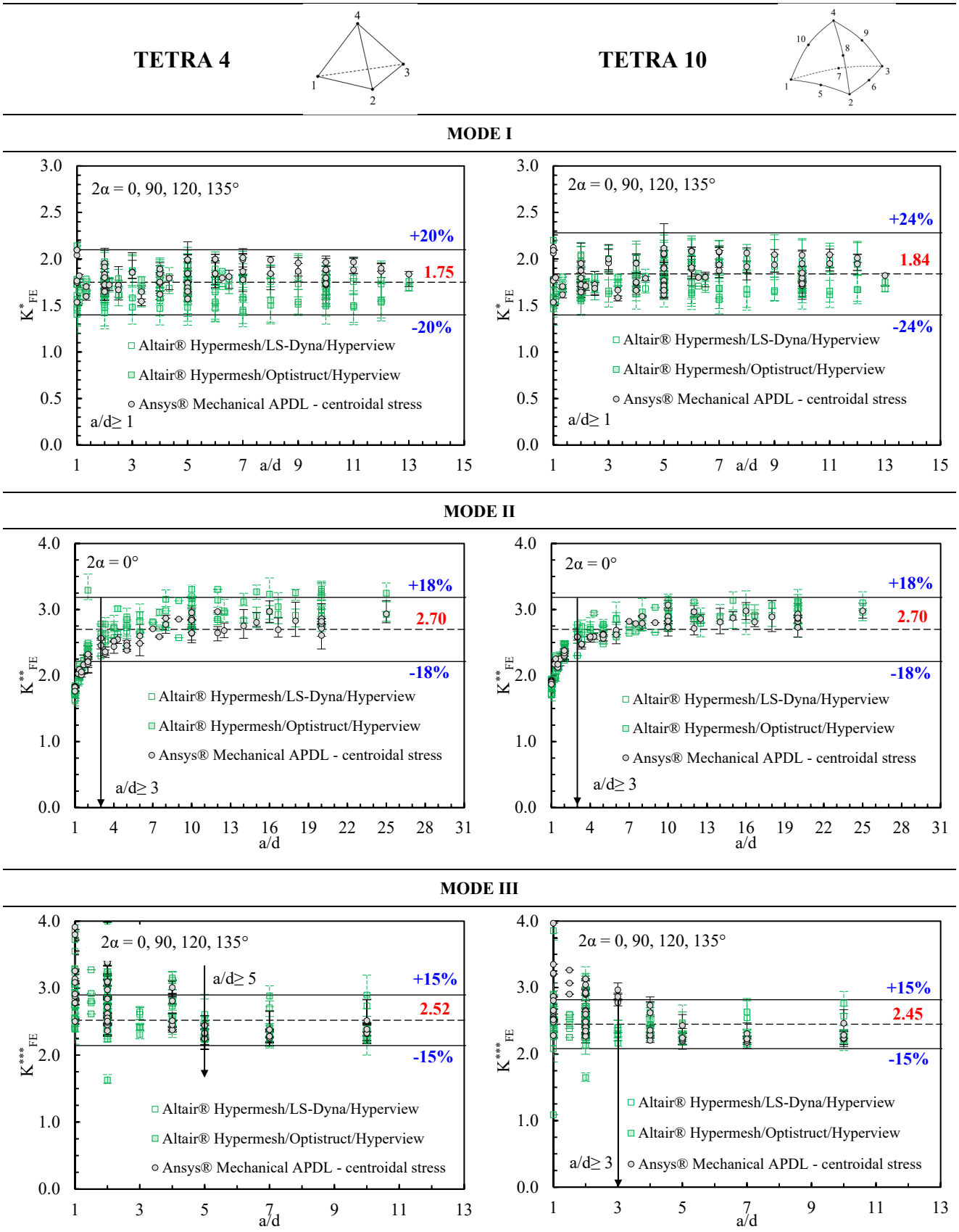

Figure 8: Non-dimensional parameters K^{*}_{FE}, K^{**}_{FE} and K^{***}_{FE} for Ansys® Mechanical APDL and for Altair® Hypermesh/LS-Dyna/Hyperview and Hypermesh/Optistruct/Hyperview FE packages. Results for mode I, II and III loadings based on centroidal stresses (according to Fig. 7b). The scatter bands have previously been calibrated in Figs. (4)-(6) on LS-dyna results.

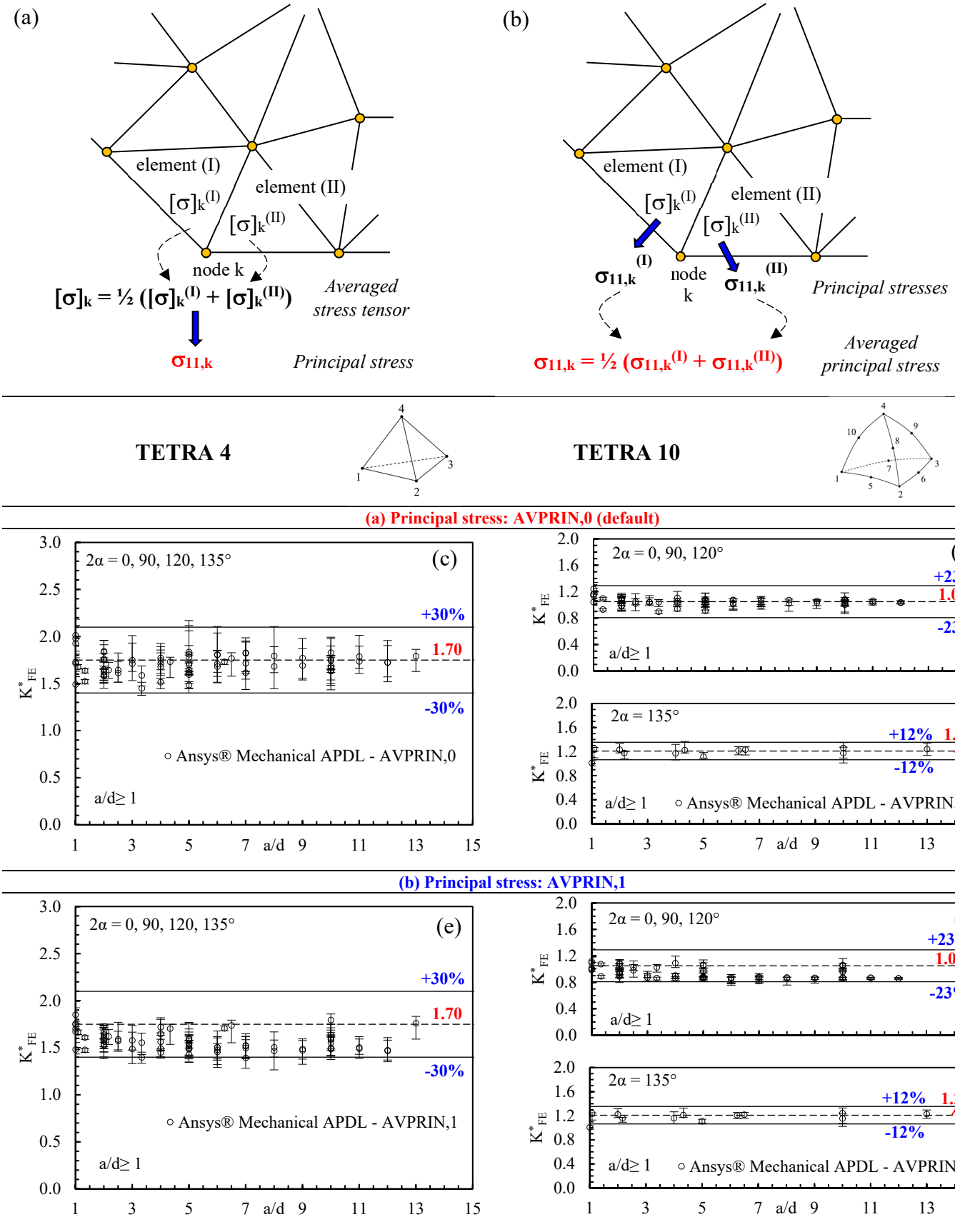

Figure 9: Principal stress averaging options. (a) Principal stresses from average stress tensor. (b) Principal stresses from element principal stresses. Non-dimensional parameter K^*_{FE} for Ansys® Mechanical APDL. Results for mode I loading obtained by adopting principal stress averaging option (a) in figures (c),(d) and option (b) in figures (e),(f). The scatter bands have previously been calibrated in Fig. (4) using the opening peak stress $\sigma_{\theta\theta,\theta=0,peak}$.

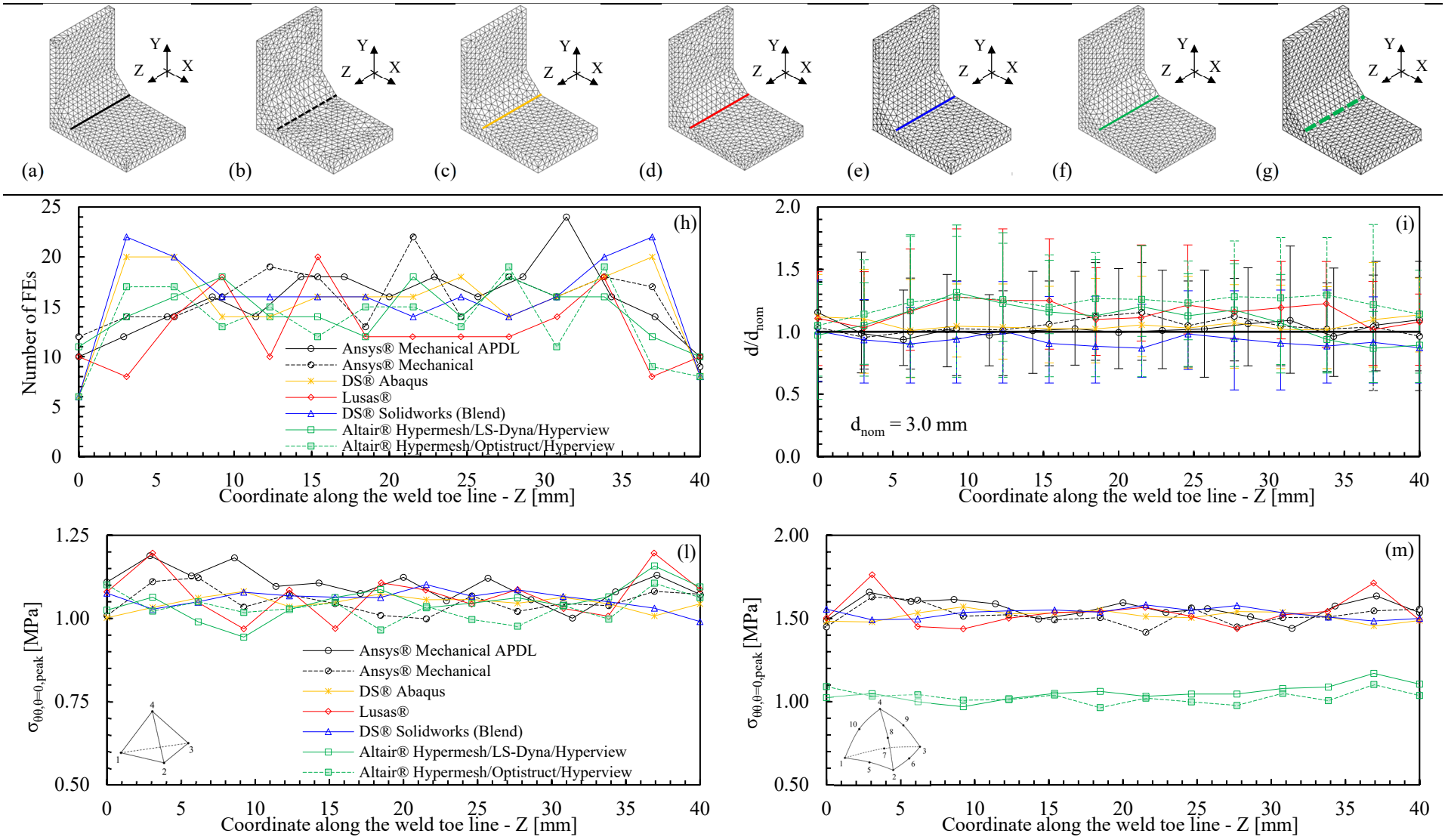

Figure 10: FE mesh patterns relevant to the case of Fig. 3d with 2a = 13 mm, 2α = 135°, and d = 3 mm, as obtained with: (a) Ansys Mechanical APDL, (b) Ansys Mechanical, (c) Abaqus, (d) Lusas, (e) Solidworks, (f) Hypermesh/LS-Dyna/Hyperview and (g) Hypermesh/Optistruct/Hyperview. (h) Number of finite elements that share each vertex node at the weld toe. (i) Normalized size of finite elements that share each vertex node at the weld toe. Comparison of peak stress distributions calculated by all considered FE codes along the weld toe line of the FE models reported in figures (a)-(g) using (l) four-node and (m) ten-node tetra elements.

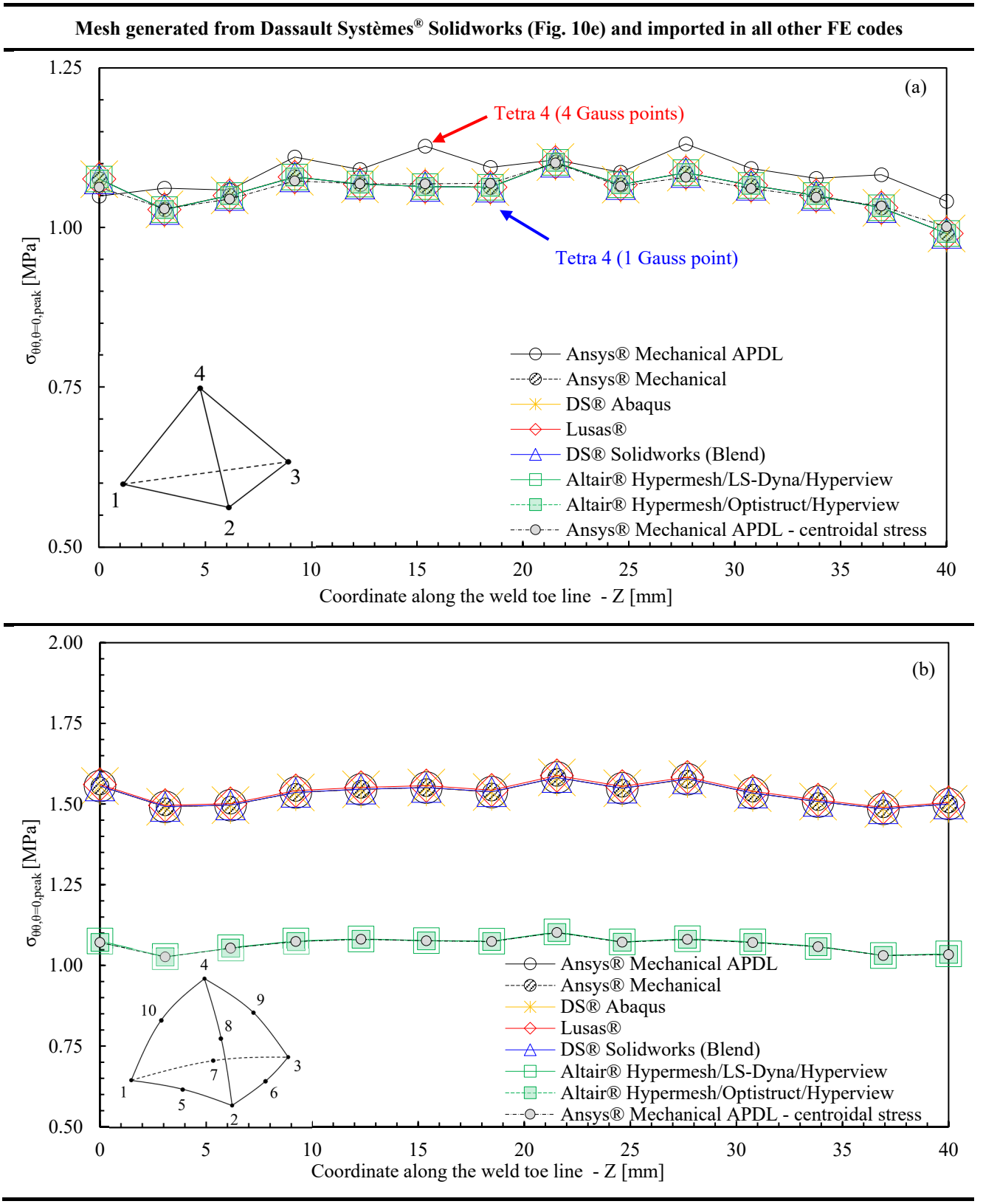

Figure 11: Comparison of peak stress distributions calculated by all considered FE codes along the weld toe line of the FE mesh pattern relevant to the case of Fig. 3d with 2a = 13 mm, 2α = 135°, and d = 3 mm, as generated by Solidworks (see Fig. 10e) adopting (a) four-node and (b) ten-node tetra elements, respectively.

TABLES

Table 1: Parameters depending on the notch opening angle 2α.

2α (°)	λ_1 [(a)]	λ_2 [(a)]	λ_3 [(b)]
0	0.500	0.500	0.500
90	0.545	0.909	0.667
120	0.616	-	0.750
135	0.674	-	0.800

[(a)]: values derived from Williams[33]
[(b)]: values derived from Qian and Hasebe[34]

Table 2: FE codes, list of partecipants and information on the adopted element types and related meshing options.

Software	**UNI**	**Version**	**TETRA 4**		**TETRA 10**		**Meshing options**	
			Element type	*Gauss points*	*Element type*	*Gauss points*	*Mesh pattern*	*Other*
Ansys® Mechanical APDL	UniBO	17.1	SOLID285	4	SOLID187	4	Free	n.a.
	UniGE	??						
	UniPA	18.1						
	UniPD	2019 R1						
	UniPI	2019 R1						
	UniTN	17.2-18.1						
Ansys® Mechanical*	UniPD	2020 R2	SOLID185	1	SOLID187	4	Free	n.a.
Dassault Systèmes® Abaqus	UniSA	6.14-1	C3D4	1	C3D10	4	Free	Equi triangle
	UniCampania							
	UniPR	2019					Free	Equi triangle
Lusas®	UniMoRe	V17 (edu)	TH4	1	TH10	4	Free	n.a.
Dassault Systèmes® Solidworks	UniMoRe	2018	Draft	1	High	4	Standard (quasi-mapped)	(a) Right triangle
	UniMoRe & UniPD	2020					Blend (free)	(b) Equi triangle
Altair® Hypermesh/ LS-Dyna/Hyperview	PoliTO	2019[(a)] R9[(b)]	EQ-10	1	EQ-17	4	Free	n.a.
Altair® Hypermesh/ Optistruct/Hyperview	UniGe	2019	EQ-10	1	EQ-17	4	Free	n.a.

* available within Ansys Workbench environment
[(a)] Altair® Hyperworks 2019 (Hypermesh / Hyperview) version; [(b)] LS-Dyna R9 version (2017)
n.a. = not applicable

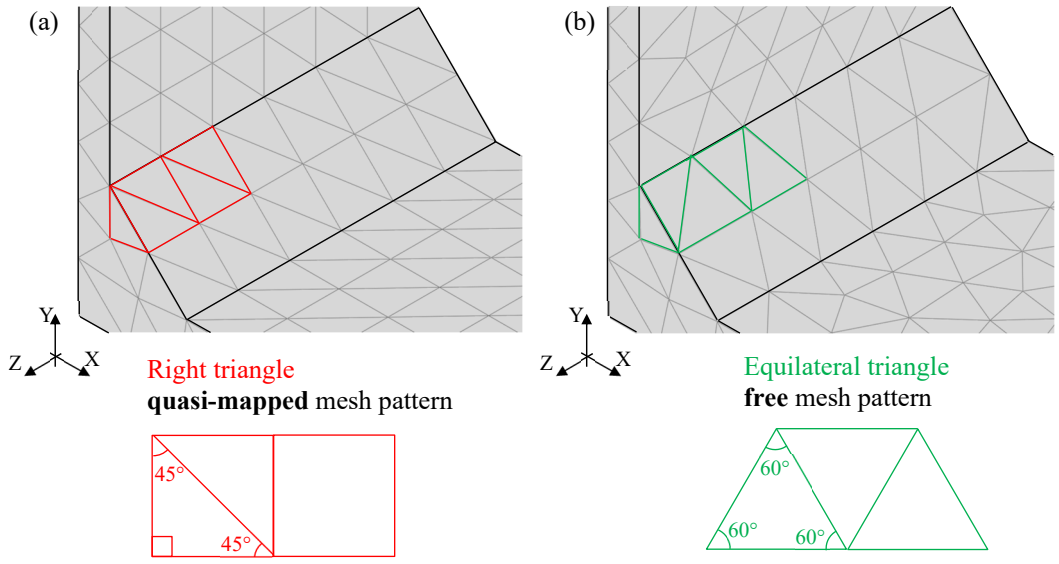

Table 3: FE analyses of 3D geometries under mode I, II and III loadings.

Mode I						
Figure	**a [mm]**	**d [mm]**	**2α [°]**	**b [mm]**	**t [mm]**	**Number of analyses***
(3a)	1, 2,…,9, 10	1	0	-	-	10
(3b)	1, 2,…,19, 20	1	0	-	-	20
(3b)	10	2, 5, 10	0	-	-	3
(3c)	5	1, 2, 2.5, 5	90	-	-	4
(3c)	10	1, 2.5, 3, 5, 7.5	90	-	-	5
(3c)	15	1, 2, 5	90, 120	-	-	6
(3c)	5	1, 2, 2.5, 5	120	-	-	4
(3c)	10	1, 2.5, 3, 5, 7.5	120	-	-	5
(3c)	10	1, 2.5, 5, 10	135	-	-	4
(3d)	6.5	0.5, 1, 1.5, 3, 6.5	135	10	8	5
(3d)	50	2, 5, 8, 10	135	50	16	4
Mode II						
Figure	**a [mm]**	**d [mm]**	**2α [°]**	**b [mm]**	**t [mm]**	**Number of analyses****
(3e)	3	3	0	-	-	1
(3e)	4	3, 4	0	-	-	2
(3e)	5	3, 4, 5	0	-	-	3
(3e)	6	3, 4, 6	0	-	-	3
(3e)	7	3.5, 7	0	-	-	2
(3e)	8	4, 6, 8	0	-	-	3
(3e)	9	3, 4.5, 6	0	-	-	3
(3e)	10	3, 5, 10	0	-	-	3
(3e)	20	4, 5, 6, 10	0	-	-	4
(3e)	30	3, 5, 7, 10	0	-	-	4
(3e)	40	4, 5, 8, 10	0	-	-	4
(3e)	50	3, 5, 10	0	-	-	3
(3e)	60	3, 4, 5, 8, 10	0	-	-	5
(3e)	70	3.5, 5, 10	0	-	-	3
(3e)	80	4, 5, 8, 10	0	-	-	4
(3e)	90	4.5, 5, 7.5, 10	0	-	-	4
(3e)	100	4, 5, 8, 10	0	-	-	4
Mode III						
Figure	**a [mm]**	**d [mm]**	**2α [°]**	**Φ [mm]**	**l_{sp} [mm]**	**Number of analyses*****
(3f)	5	1, 2.5, 5	0, 90, 120, 135	50	-	12
(3f)	7	1, 3.5, 7	0, 90, 120, 135	50	-	12
(3f)	10	1, 2.5, 5	0, 90, 120, 135	50	-	12
(3g)	5	5	90, 120, 135	50	-	3
(3g)	10	5, 10	90, 120, 135	50	-	6
(3g)	15	5, 10	90, 120, 135	50	-	6
(3h)	2	2	0	50	4	1
(3h)	5	2.5, 5	0	50	10	2
(3h)	10	2.5, 5	0	50	20	2

*: total number of analyses: 70 x 2 element types (TETRA 4 and TETRA 10) = 140 analyses
**: total number of analyses: 55 x 2 element types (TETRA 4 and TETRA 10) = 110 analyses
***: total number of analyses: 56 x 2 element types (TETRA 4 and TETRA 10) = 112 analyses

Table 4. Summary of parameters K^{*}_{FE}, K^{**}_{FE} and K^{***}_{FE} and minimum mesh density ratios *a*/*d* to apply the PSM with all considered FE codes using either four-node or ten-node tetra elements.

Software	**PSM parameter**	**Mode I – K^{*}_{FE} (Eq. (8))**			**Mode II – K^{**}_{FE} (Eq. (9))**		**Mode III – K^{***}_{FE} (Eq. (10))**		
		TETRA 4	**TETRA 10**		**TETRA 4**	**TETRA 10**	**TETRA 4**	**TETRA 10**	
	2α [°]	**0, 90, 120, 135**	**0, 90, 120**	**135**	**0**	**0**	**0, 90, 120, 135**	**0, 90**	**120, 135**
Ansys® Mechanical APDL *original calibration*[47]	K_{FE}	1.75±22%	1.05±15%	1.21±10%	2.65±15%	1.63±20%	2.50±15%	1.37±15%	1.70±10%
	$(a/d)_{min}$	3	3	1	3	1	5	3	3
Ansys® Mechanical APDL	K_{FE}	1.70±30%	1.05±23%	1.21±12%	2.63±18%	1.61±20%	2.47±15%	1.40±15%	1.68±10%
	$(a/d)_{min}$	1	1	1	3	1	5	3	1
Ansys® Mechanical	K_{FE}	1.75±18%	1.05±18%	1.21±8%	2.90±15%	1.63±15%	2.47±18%	1.32±12%	1.63±10%
	$(a/d)_{min}$	1	1	1	3	1	5	3	1
Dassault Systèmes® Abaqus	K_{FE}	1.75±18%	1.05±18%	1.21±8%	2.72±15%	1.63±15%	2.35±20%	1.35±12%	1.60±12%
	$(a/d)_{min}$	1	1	1	3	1	5	5	4
Lusas®	K_{FE}	1.78±18%	1.07±15%	1.20±10%	2.87±15%	1.63±15%	2.48±16%	1.40±12%	1.65±12%
	$(a/d)_{min}$	1	1	1	3	1	5	3	1
Dassault Systèmes® Solidworks *	K_{FE}	1.72±18%	1.05±18%	1.21±8%	2.65±12%	1.61±13%	2.35±15%	1.37±10%	1.70±12%
	$(a/d)_{min}$	1	1	1	3	1	5	3	1
Altair® Hypermesh/ LS-Dyna/Hyperview	K_{FE}	1.75±20%	1.84±24%	1.84±24%	2.70±18%	2.70±18%	2.52±15%	2.45±15%	2.45±15%
	$(a/d)_{min}$	1	1	1	3	3	5	3	3
Altair® Hypermesh/ Optistruct/Hyperview	K_{FE}	1.68±25%	1.80±22%	1.80±22%	3.00±18%	2.87±15%	2.60±23%	2.50±18%	2.50±18%
	$(a/d)_{min}$	1	1	1	3	3	5	1	1

***** using *Blend* mesh generation option (see Table 2)

Table 5: Options for principal stress averaging available in the considered FE codes.

FE Software	Averaging option (a) of Fig. 9	Averaging option (b) of Fig. 9
Ansys® Mechanical APDL	AVPRIN,0 or "from components" (*default*)	AVPRIN,1 or "from principals"
Ansys® Mechanical	*default*	*not available*
Dassault Systèmes® Abaqus	"compute scalars after averaging"	"compute scalars before averaging" (*default*)
Lusas®	Averaged nodal (*default*)	*not available*
Dassault Systèmes® Solidworks	*default*	*not available*
Altair® Hypermesh/ Hyperview*	Averaging method: "Advanced"	Averaging method: "Simple" (*default*)

***** Post-processor adopted to calibrate both Altair® LS-Dyna and Altair® Optistruct